

RESEARCH

Open Access



A Unified Formula for Calculation of Crack Width and Spacing in Reinforced Concrete Beams

Xianhua Yao¹, Junfeng Guan^{1*} , Lei Zhang², Junyi Xi¹ and Lielie Li¹

Abstract

Crack distribution and widths were experimentally examined in a series of reinforced concrete (RC) beams. Concretes of different strengths were used, and beams were reinforced with 600 MPa yield strength steel bars. The features of cracks, which need to be considered in the design, were determined by using statistical analysis of different crack patterns observed in RC beams. The methods for determining the depth of effective influence zone of 600 MPa steel bars in RC beams were experimentally obtained. Based on the experimental data obtained in this study and from the data on RC beams with 335–600 MPa yield strength steel bars from other studies, the applicability of different formulas for the determination of the maximum widths (provided in codes and by scholars) was analyzed. Methods for the calculation of average crack spacing and maximum crack widths in RC beams with steel bars of various yield strengths were proposed. A unified formula for the calculation of maximum crack width in such beams was also established.

Highlights

- Reinforced concrete beam cracking behavior was experimentally examined with a new type of seismic bar.
- New methods for the calculation of average crack spacing and maximum crack width were presented.
- A unified formula for the calculation of maximum crack width was proposed.

Keywords: crack width, crack spacing, reinforced concrete beam, 600 MPa steel bar, concrete strength

1 Introduction

Checking and controlling of cracks in reinforced concrete (RC) components or structures are the key issues in the engineering design, construction, and serviceability of concrete structures. In particular, crack control is a major factor in design when high-strength steel bars are used. An accurate crack width checking is known as a crucial and complicated problem in the design and testing of RC

structures (Beeby, 2004; Frosch, 2002; Guan, 2010; Guan et al. 2011; Zhao et al. 2008, 2009). Therefore, a correct establishment of the crack width checking approach for RC structures is theoretically significant and offers a practical value in structural engineering. Existing formulas for crack width checking in RC beams differ among countries, they are inconsistent, and can be roughly divided into two types. The first type is semi-theoretical and semi-empirical formulas, which are based on the analysis of the cracking mechanism, and are theoretically derived on the basis of mechanical models. However, some of the coefficients in them are determined from experiments or experience. Formulas belonging to the first type can be found in the US codes ACI318-99

*Correspondence: junfengguan@ncwu.edu.cn

¹ School of Civil Engineering and Communication, North China University of Water Resources and Electric Power, Zhengzhou 450045, Henan, China
Full list of author information is available at the end of the article
Journal information: ISSN 1976-0485 / eISSN 2234-1315

(ACI Committee, 1999) and ACI318-14 (ACI Committee, 2014), European norm EN 1992-1-1 (EN1992-1-1, 2004), and Chinese codes GB (GB50010, 2010), DL/T (DL/T 5057-1996, 1996; DL/T 5057-2009, 2010) and SL/T (2009). The second type is formulas based on mathematical statistics, which involves conducting a regression analysis of the impacts of different parameters on the crack width development and requires a large number of measured data. After selecting the most important parameters, an appropriate mathematical statistics methodology is used to directly establish an appropriate formula. Such examples are formulas provided in the US codes ACI318-71 (ACI Committee, 1971) and ACI318-95 (ACI Committee, 1995), and Chinese codes JTG (JTGD62-2012, 2012), JTJ (JTJ267-98, 1998) and TB (TB10002.3-2005, 2005).

In the current Chinese codes for the design of concrete structures (e.g., GB50010 for civil engineering concrete structures (GB50010, 2010), DL/T 5057 and SL/T 191 for hydraulic concrete structures (DL/T 5057-1996, 1996, DL/T 5057-2009, 2010; SL/T 191-2008, 2009), JTG D62 for highway RC structures (JTG D62-2012, 2012), JTJ 267 for harbor engineering concrete structures (JTJ267-98, 1998), and TB10002.3 for railroad RC structures (TB10002.3-2005, 2005)), the highest yield strength of ordinary steel bars is 500 MPa, which can also be considered as a standard value. However, the highest yield strength of ordinary steel bars specified in ACI 318-14 (ACI Committee, 2014) and EN 1992-1-1 (EN1992-1-1, 2004) is 550 and 600 MPa, respectively. Application of high-strength steel bars with yield strength of 600 MPa in RC structures reduces steel consumption and represents a new economical and efficient design approach. Furthermore, their performance during the seismic action turned out to be satisfying. In China, studies of the performance of high-strength steel bars with yield strength of 600 MPa and their structural and mechanical properties are still in an early stage (Guan et al., 2016, 2018). Zhao et al. (2008) put forward the statistical analysis principle of crack classification of 335 MPa reinforced concrete beams and made statistical calculation and analysis. According to the statistical analysis, the average crack spacing, average crack width, and distribution model of crack width were evaluated. Liu et al. (2019) investigated the effect of carbon fiber composite (CFRP) reinforcement on crack growth, evolution characteristics, and fractal dimensions of prestressed concrete beams under concentrated loads. The test results show that CFRP has an inhibitory effect on the cracks. The crack width conforms to the normal distribution. The scattering coefficient, average width, and characteristic width decreased with the increase in height. The three parameters of the CFRP-strengthened beam with the same height were smaller than those of the

unreinforced beam. Du and Su (2012) performed a statistical analysis on the crack widths at different positions of post-tensioned bonded prestressed concrete beams with 500 MPa steel bars. The results indicated that the crack width at each position follows the normal distribution, and the short-term crack width expansion coefficient at each position is the same. Li et al. (2019) studied the shear performance of steel fiber reinforced expanded-shale lightweight concrete (SFRELC) beams without mesh reinforcement. According to the basic design principles and experimental results, statistical analysis of the shear crack resistance, shear crack distribution and width, mid-term deflection, shear failure mode, and shear capacity of the specimens was carried out. The research showed that steel fibers could effectively enhance the shear performance of reinforced SFRELC beams without net reinforcement. Yao et al. (2020) tested the flexural capacity of concrete beams with varying strength grades and different reinforcement ratios embedded with new 600 MPa-grade steel bars. The research showed that when the measured values of yield strength of reinforcement and concrete strength were adopted, the ratio of measured failure moment value to calculated value of each beam based on different codes was close to 1.0. In addition, according to the reliability analysis, the design yield strength of 600 MPa-grade high-strength steel bars should be 520 MPa. Li et al. (2018) carried out an experimental study on 600 MPa reinforced concrete columns under axial compression. It was demonstrated that the 600 MPa steel bar as longitudinal reinforcement had little influence on the strength, but when it was used as the stirrup, the concrete columns showed better strength, deformation and toughness. Zhang et al. (2019) found that HRB600 reinforced high-strength concrete columns had better recoverability after the earthquakes with good hysteretic performance and energy dissipation capacity. In addition, Zhang et al. (2021) studied the seismic performance of reinforced shear walls with HRB600 and confirmed that the 600 MPa reinforced shear wall had stable hysteretic behavior, while HRB600 reinforced shear wall could reduce the residual deformation better than HRB400 reinforced shear wall. Xiong et al. (2018) evaluated the mechanical properties of HRB600 steel bar. It was concluded that the design value of tensile yield strength of HRB600 steel bar should be taken as 520 MPa. Guan et al. (2018) tested the mechanical properties of new 600 MPa-grade seismic steel bars. The study showed that the strength and deformation properties meet the requirements of Chinese and foreign seismic design standards. The measured values of the yield and the ultimate tensile strengths were larger than 630 and 800 MPa, respectively, and the maximum total elongation A_{gt} exceeded 9%. Based on the test data, mathematical

expression for tensile constitutive relation was proposed for 600 MPa-grade seismic steel bars. Furthermore, Guan et al. (2016) carried out the research on the anti-crack performance of reinforced concrete beams with 600 MPa-grade steel bars, and presented a correction formula for the crack calculation when such bars are used. Guan et al. (2021) examined the mid-span deflection of reinforced concrete beams with high strength of 600 MPa and its calculation method. The test results showed that the strain change of concrete beams with high strength of 600 MPa was as per the assumption of the plane section, and the full curve of load-mid-span deflection is a triple line. A unified calculation method was established for the mid-span deflection of concrete beams with different strengths with 335–600 MPa steel bars. Guan et al. (2020) conducted stiffness tests on beams with 600 MPa high-strength steel bars, and C60 high-strength concrete with 600 MPa-grade steel bars had excellent deformation behavior, and improved ultimate bearing capacity of the beams. Three models for stiffness of beams with 600 MPa high-strength steel bars and high-strength concrete were recommended. Unfortunately, a relatively limited research has been focused on the crack width of concrete specimens reinforced with 600 MPa-grade high-strength steel bars. Therefore, it should be experimentally checked whether the crack width verification formulas recommended by existing structural design standards can be applied in cases of concrete beams with 600 MPa-grade steel bars.

This paper presents the results of the crack width tests performed on a series of beams made out of concretes with different strengths and 600 MPa high-strength steel bars. Additionally, the regularity of crack distribution and width during serviceability conditions were also investigated. Crack widths were determined through the statistical analysis of the obtained data. An approach for the determination of the effective tension-affected zone was proposed based on the experimentally obtained results.

The existing calculation approaches for RC beams that provide crack spacing and width checking formulas were evaluated by using the experimental results of this study, in which 335–500 MPa-grade steel bars were used, and average crack spacing and maximum crack widths were investigated. Finally, methods for the calculation of average crack spacing and maximum crack widths were presented, and a unified formula for the maximum crack width was proposed for beams with 335–600 MPa-grade steel bars.

2 Experimental Study on RC Beams with 600 MPa Steel Bars

2.1 Materials

Four different concrete mixtures were used in the study, denoted by C30, C40, C50 and C60. The basic properties of the materials used to develop the four types of concrete are shown in Table 1. The detailed proportions of concrete mixtures can be found in Table 2.

Experimentally determined mechanical properties of concrete are listed in Table 3. At the same age of every batch of experimental RC beams, six identical cubes with the side length of 150 mm were prepared, to determine the compressive strength f_{cu} and the splitting tensile strength f_{ts} (both as average values from three cubes). Meanwhile, six identical prisms with the dimensions of 150 × 150 × 300 mm were prepared in every batch and tested to obtain the elastic modulus E_c and compressive strength f_c (both as average values from three prisms).

In this study, 600 MPa steels bars (Guan et al., 2021) were used as the longitudinal reinforcement in RC beams. The experimentally determined stress–strain curves for 600 MPa steel bars are shown in Fig. 1. The stress–strain full curves of the 600 MPa class steel bars showed obvious yielding steps in three stages, namely, elasticity, yield, and stress strengthening. The experimentally obtained mechanical properties of 600 MPa-grade steel bars (average values) are listed in Table 4. The actual yield strengths

Table 1 The physical properties of materials used in configuring concrete

Mixture	Cement (General Administration of Quality Supervision, Inspection and Quarantine; and National Standardizing Committee 2007)			Fine aggregate	Coarse aggregate		Slump (mm)
	Type	28d compressive strength(MPa)	Apparent density (g/cm ³)	Apparent density (kg/m ³)	Apparent density (kg/m ³)	Bulk density (kg/m ³)	
C30	P-O 42.5	49.4	3.043	2700	2710	1630	120~200
C40							
C50	P-O 52.5	57.7	3.244				
C60							

Table 2 Concrete mixture proportion.

Mixture	Cement, (kg/m ³)	Water, (kg/m ³)	w/c	Aggregate (kg/m ³)			Sand (kg/m ³)	High-range water reducing admixture (kg/m ³)
				5 to 10 (mm)	10 to 16 (mm)	16 to 20 (mm)		
C30	378 (No.42.5)	189	0.50	491	328	273	758	1.89
C40	473 (No.42.5)	189	0.40	491	328	273	670	3.31
C50	473 (No.52.5)	189	0.40	491	328	273	698	3.31
C60	630 (No.52.5)	189	0.30	458	305	254	624	5.04

Table 3 Experimental mechanical properties of concrete.

Mixture	f_{cu} (MPa)	f_{ck} (MPa)	f_{ts} (MPa)	$E_c \times 10^4$ (MPa)	Age (days)	Batch number
C30	37.7	26.4	2.0	3.8	200	1
C40	42.6	32.3	2.7	3.7	250	2
C50	53.0	33.3	3.4	3.7	260	3
C60	66.3	61.8	3.3	4.1	290	4
C60	67.1	62.3	3.4	4.1	300	5

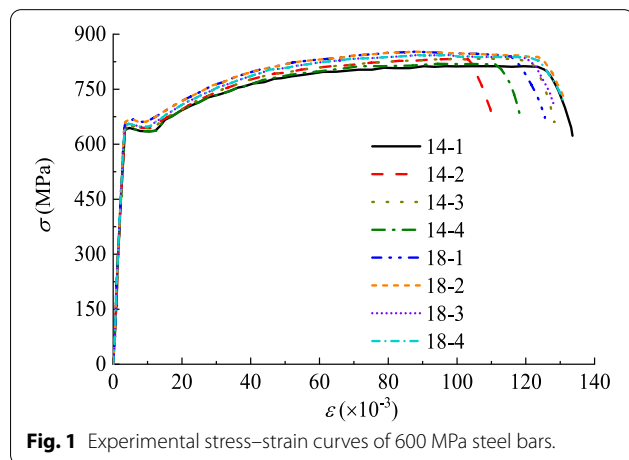


Fig. 1 Experimental stress–strain curves of 600 MPa steel bars.

Table 4 Experimental mechanical properties of 600 MPa steel bars.

Diameter d (mm)	Yield strength f_y (MPa)	Ultimate strength f_u (MPa)	f_u/f_y	Elastic modulus E_s (GPa)	Maximum force total elongation A_{gt} (%)
14	635.71	819.92	1.29	198	10.03
18	645.02	840.38	1.30	195	10.13

f_y of bars with different diameters d ranged from 634.17 to 648.38 MPa, and the corresponding ultimate strengths ranged from 808.15 to 843.20 MPa. The values measured

in each tested group were relatively close, and the dispersion coefficient was small.

In the US code ASTM A706 (ASTM A706/A706M-14, 2014), the ratio of ultimate tensile strength f_u to yield strength f_y of steel bars is specified to be $f_u/f_y = 1.25$. European standard EN 1992-1-1 (EN1992-1-1, 2004) sets the f_u/f_y ratio in the range of 1.05 to 1.35. For the seismic design of RC members, Chinese standard GB50010 (GB50010, 2010) requires that the f_u/f_y ratio should not be less than 1.25. Experimentally measured values of the f_u/f_y ratio of 600 MPa-grade steel bars considered in this study were in the range of 1.27–1.31.

European standard EN1992-1-1 (EN 1992-1-1, 2004) specifies that the characteristic strain at maximum force of C-grade steel bars should be larger than 7.5%. For the seismic design of RC members, Chinese standard GB50010 (GB50010, 2010) specifies that the measured elongation of steel bars at maximum force (A_{gt}) should not be less than 9%. The measured values A_{gt} of 600 MPa-grade steel bars were larger than 9%.

Therefore, the strength and deformation properties of the applied 600 MPa steel bars met the requirements of the Chinese standard GB50010 (GB50010, 2010), the US code ASTM A706 (ASTM A706/A706M-14, 2014) and the European standard EN 1992-1-1 (EN1992-1-1, 2004).

2.2 Design of RC Beams

Eight groups of 16 RC beams with 600 MPa steel bars, in which different concrete strength and reinforcement ratios were used, were cast for the experiment and were denoted as C30-1, C30-2, C40-1, C40-2, C50-1, C50-2,

C60-1 and C60-2. For comparison, two additional RC beams with 400 MPa steel bars were also cast, and were denoted by CR60-1 and CR60-2, to be associated with the C60-1 group.

The geometry of the RC beams is shown in Fig. 2, in which b denotes width, h denotes depth, l_0 represents the span, and c is the concrete cover. h_0 is the effective depth, determined as $h_0 = h - a_s = h - c - d/2$, where a_s denotes the distance from the concrete face to the center of gravity of steel bars.

The details of RC beams with 600 and 400 MPa steel bars are listed in Table 5, where ρ denotes the

reinforcement ratio determined as $\rho = A_s / (bh_0)$, and A_s is the area of steel bars.

2.3 Test Setup

As shown in Fig. 3, tested beams were loaded in reverse to clearly observe the cracks. Two points at the mid-span section were symmetrically loaded to form an 800 mm purely bent section. The load intensity was based on the design bending moment of the purely curved section. The static loading was applied by considering the effects of the beam and loading equipment self-weights. Loading

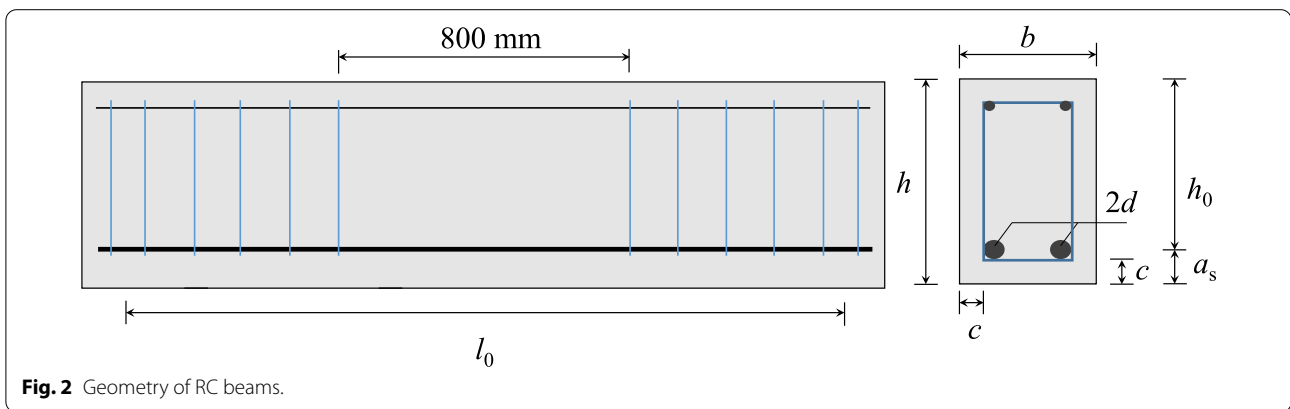


Fig. 2 Geometry of RC beams.

Table 5 Details of RC beams.

RC beams number	Width b (mm)	Depth h (mm)	Effective span l_0 (mm)	Concrete cover c (mm)	Reinforcement details		Reinforcement rate ρ (100%)	Batch number
					Numbers of bars	Bar diameter d (mm)		
C30-1-1	200	350	2550	30	2	18	0.008	1
C30-1-2	200	350	2550	30	2	18	0.008	1
C30-2-1	200	350	2550	30	2	14	0.005	1
C30-2-2	200	350	2550	30	2	14	0.005	1
C40-1-1	200	350	2550	30	2	18	0.008	2
C40-1-2	200	350	2550	30	2	18	0.008	2
C40-2-1	200	350	2550	30	2	14	0.005	2
C40-2-2	200	350	2550	30	2	14	0.005	2
C50-1-1	200	350	2550	30	2	18	0.008	3
C50-1-2	200	350	2550	30	2	18	0.008	3
C50-2-1	200	350	2550	30	2	14	0.005	3
C50-2-2	200	350	2550	30	2	14	0.005	3
C60-1-1	200	350	2550	30	2	18	0.008	5
C60-1-2	200	350	2550	30	2	18	0.008	5
C60-2-1	200	350	2550	30	2	14	0.005	4
C60-2-2	200	350	2550	30	2	14	0.005	4
CR60-1-1	200	350	2550	30	2	18	0.008	5
CR60-1-2	200	350	2550	30	2	18	0.008	5

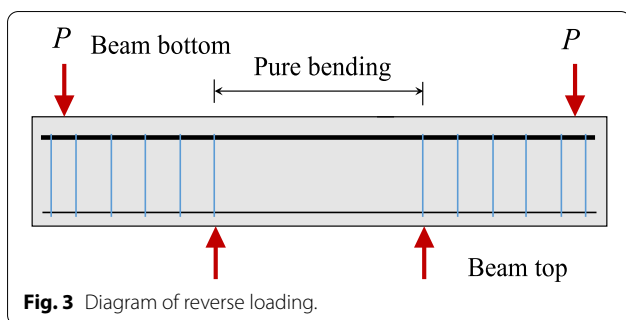


Fig. 3 Diagram of reverse loading.



Fig. 4 Actual RC beams with 600 MPa steel bars and test device.

intensities at all levels were controlled by readings of the data acquisition system connected to sensors.

The tested RC beams with 600 MPa steel bars and test setup are shown in Fig. 4. To clearly observe the cracks and determine the crack width values of the side and bottom surfaces of the test beam, the test beam was reversely loaded. The strain gauge measuring points were symmetrically arranged along both sides of the beam. The load values of each level were controlled by a data acquisition system connected to a sensor. During formal loading, systematic loading was applied according to the calculated ultimate load. Before the specimen was cracked, the load increment for each level was 10% of the calculated cracking load. When it reaches 90% of the cracking load, the load increment for each level was reduced to accurately obtain the cracking load of the specimen. Each stage was loaded for 10–15 min, and the corresponding data were recorded until the load on the test beam reached the maximum value.

In the test, the loads which initiated cracking were observed and recorded, along with the width and depth of the corresponding cracks. The distribution of cracks under serviceability-level loads was studied. The values of

crack widths on the surface of beams that corresponded to the center of gravity of the longitudinal steel bars were measured during the test to establish methods for the calculation of the crack width at the center of gravity of the RC beams with 600 MPa reinforcement. The widths of various cracks that formed at different heights of the specimens were measured to determine the effective tension-affected zone of the longitudinal steel bars (the measured height was na_s).

3 Analysis and Discussion of the Test Results for RC Beams with 600 MPa Steel Bars

3.1 Distribution of Cracks

Fig. 5 shows the distribution of cracks in purely bended sections of each specimen at serviceability-level loading stage. One or more cracks appeared in the weakest area of the section when the external load reached the level that initiated cracking. Cracks appeared continuously, and their width and growth increased with the increase of the load. Cracks completely erupted when the load approximately reached $0.67M_u$ (M_u denotes the ultimate bending moment).

3.2 Statistical Analysis of Crack Patterns

Cracks in RC beams are generally produced by different mechanisms and possess extended development features and width variation rules. Classification and statistical analysis of experimental results can be used to obtain relatively accurate findings. In earlier studies, the object of statistical analyses was non-uniform, and the positions of cracks observed by various researchers were different, which consequently led to large differences between the research data, and even to contradicting changing rules. Although a large research data have been accumulated, it could not be mutually verified, which ultimately affected the crack width checking methods. The crack width verification formulas provided by the current Chinese regulations are different, which actually reflects the current state of knowledge.

In this experiment, by observing the rules of various crack occurrence and extension, cracks in RC beams could be classified into four categories (Guan, 2010; Zhao et al., 2008, 2009) (see Fig. 6). Type A (main) cracks can be extended under various load levels after cracking, or can quickly grow toward the neutral axis. The causes of such cracks are the tensile stress of the steel bar at the crack interface and the increased depth of the concrete tensile zone. Type B cracks occur around the type A cracks, but no longer extend, or develop very slowly under subsequent loading, with the extension depth generally smaller than that of the type A. Such cracks belong to secondary cracks, which do not extend or develop gradually when the tensile stress of concrete cannot accumulate enough

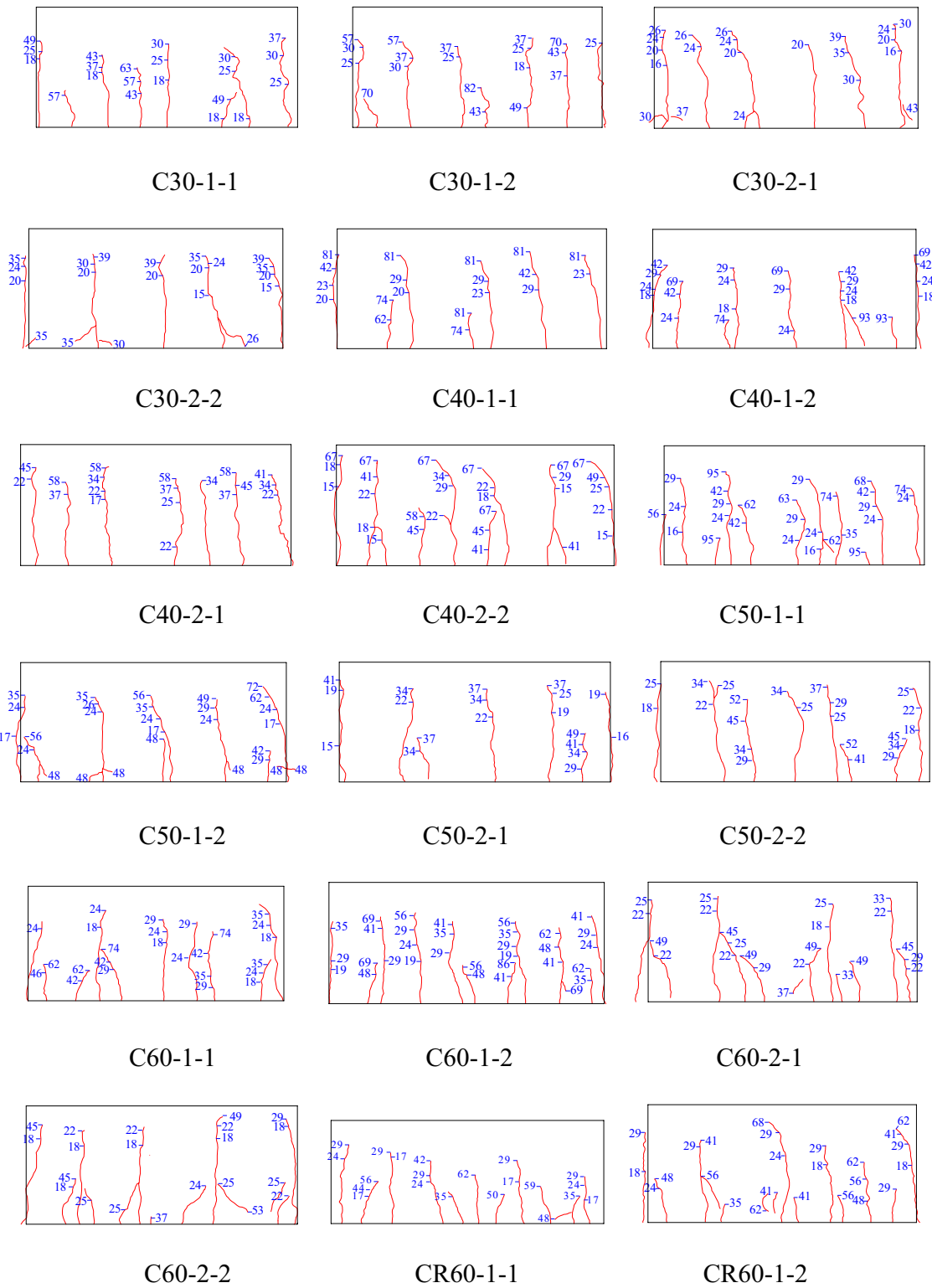
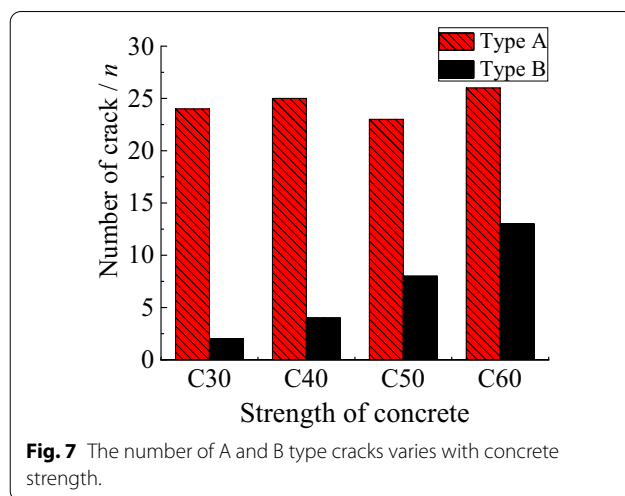
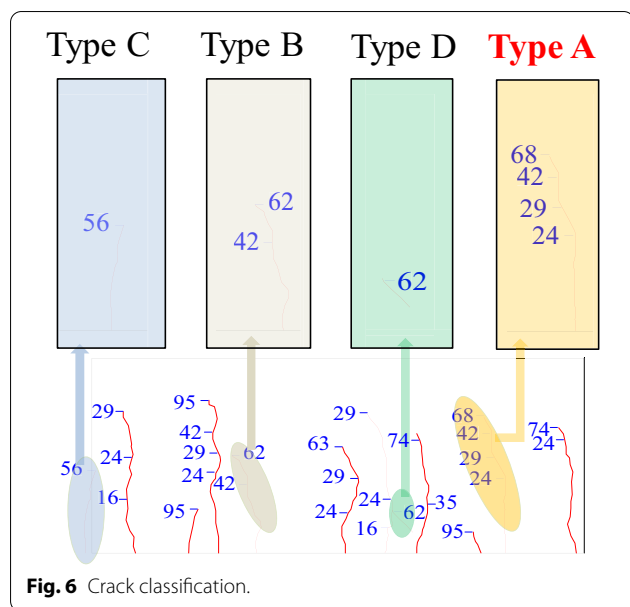


Fig. 5 Crack distribution of test RC beams (unit of value: kN).



to cause concrete cracking under the subsequent load. Type C cracks (with fracture characteristics) occur suddenly under a certain load and quickly reach a certain depth that is not developed further under subsequent loading. The primary reason for such cracks are as follows. When loaded to a certain load level, the concrete cross section between the two main cracks (whose spacing is less than twice the average crack spacing) suddenly cracks due to stress concentration caused by some defects and quickly reaches a certain depth, but does not develop any further under the action of subsequent loads. Type D (secondary) cracks occur at the center of gravity of longitudinal tensile reinforcement due to the secondary tensile stresses caused by bond slip. Type D cracks can also occur next to the type A main cracks, but the extension depth develops slowly at the longitudinal tensile reinforcement center of gravity, or at the beam bottom with the extension depth below the center of gravity of the longitudinal tensile reinforcement.

Type C and D cracks were excluded from the classification because they had low impact on the overall crack distribution and development. Statistical analysis of 135 type A and B cracks that occurred in the RC specimens with 600 MPa (125 cracks) and 400 MPa (10 cracks) reinforcing bars showed that the number of the type A cracks was basically unchanged with the increase in concrete strength, whereas the opposite was observed for the type B cracks (see Fig. 7). The type A cracks accounted for 78.52% of the total cracks, and the type B cracks accounted for the remaining 21.48%. The width of type A cracks was the largest among all crack types, and the maximum width was also observed in cracks of this type.

Therefore, the influence of the crack type on the crack mean width w_{cr} and corresponding shape properties should be determined for the crack width checking in structural design approaches.

Statistical analysis of 29 type B cracks that occurred under the considered load showed that the cracks with width smaller than w_{cr} accounted for 80.76%, cracks with width larger than w_{cr} accounted for 13.23%, and cracks with width equal to w_{cr} accounted for 6.01%. Under the subsequent load, among 29 type B cracks, the ones whose width decreased accounted for 7.2%, the ones whose width increased accounted for 75.4%, and the cracks with an unchanged width accounted for 17.4%. Cracks with width smaller than w_{cr} accounted for 86.1%, cracks with width larger than w_{cr} accounted for 12.2%, and cracks with width equal to w_{cr} accounted for 1.7%. The width of the type B cracks increased with the increase of the load, but remained unchanged with the increase of w_{cr} .

Statistical analysis of 32 cracks adjacent to type B cracks showed that cracks with decreasing width accounted for 9.7%, cracks whose width remained unchanged accounted for 15.6%, and cracks whose width increased accounted for 74.7%. The unloading effect on the part of the concrete section in tension due to the occurrence of the type B cracks exerted a certain influence on the growth of adjacent cracks on two sides. However, the width ratio of adjacent cracks increased to 85.7%, and the effects of the type B cracks were obviously reduced with the load increase.

Therefore, the average crack spacing and average and maximum crack widths, corresponding to common structural checks, were considered for the type A main cracks in the RC specimens with 600 MPa-grade reinforcing bars.

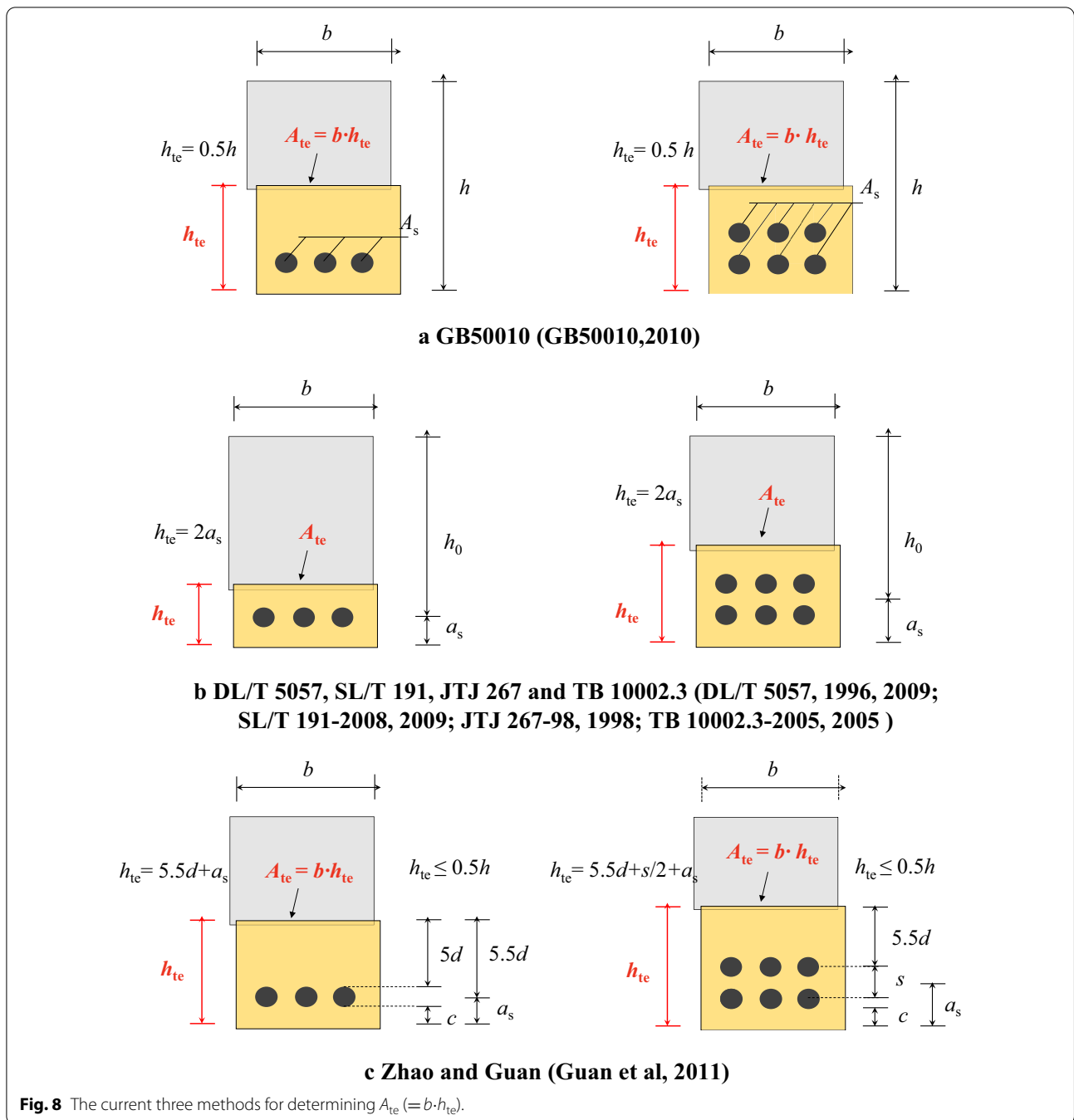


Fig. 8 The current three methods for determining $A_{te} (= b \cdot h_{te})$.

The outcomes of statistical analysis of 572 different cracks that appeared in concrete specimens with a 335 MPa-grade reinforcing bars can be found in Zhao et al. (2008), (2009) and Guan (2010). The analysis results are consistent with the ones presented in this paper. Namely, the crack shape characteristics that correspond to the crack width calculation in structural design approaches occurred due to the continuous increase of the cracked concrete tensile area depth and tensile stress

in reinforcement. Cracks continued to extend toward neutral axis. The type B cracks were the main one that controlled the overall development and distribution of cracks in beams.

3.3 Effective Tensile Area of Concrete Sections

A gripping force of longitudinal tensile reinforcement acting on surrounding concrete restricts its shrinkage on both sides of a crack, which affects the generation

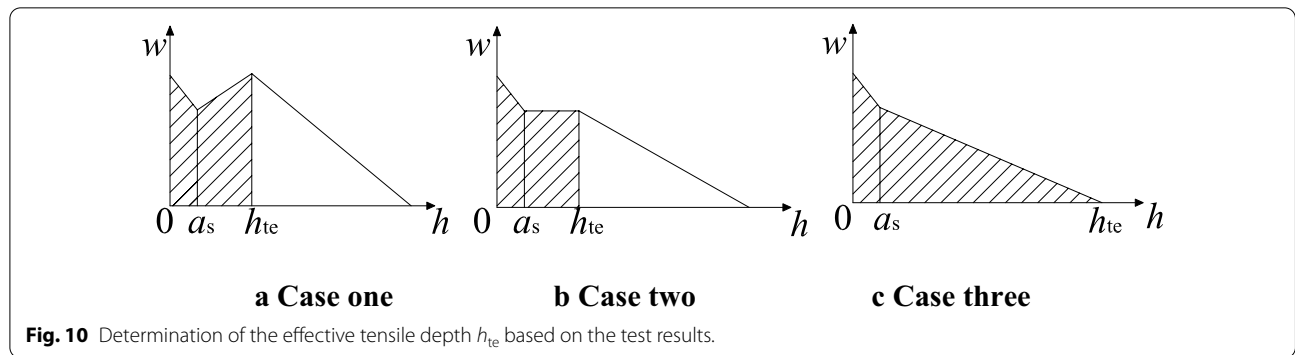
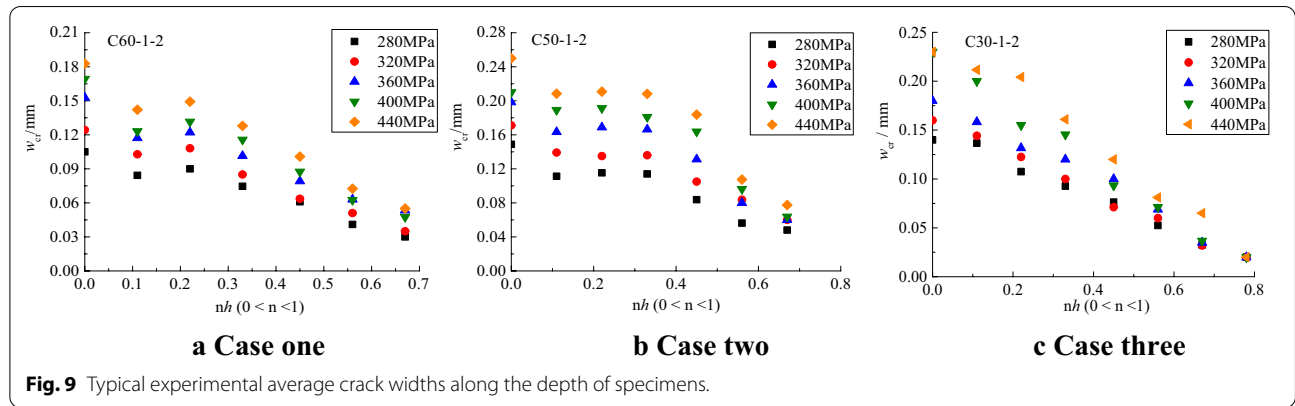


Table 6 Comparison between the experimental h_{te}^t with parameters h , a_s and d .

RC beams number	h_{te}^t/h	h_{te}^t/a_s	$(h_{te}^t-c-d)/d$
C30-1-1	0.50	4.49	7.06
C30-1-2	0.50	4.49	7.06
C30-2-1	0.21	2.00	2.14
C30-2-2	0.50	4.73	9.36
C40-1-1	0.50	4.49	7.06
C40-1-2	0.50	4.49	7.06
C40-2-1	0.50	4.73	9.36
C40-2-2	0.50	4.73	9.36
C50-1-1	0.33	3.00	3.83
C50-1-2	0.33	3.00	3.83
C50-2-1	0.32	3.00	4.79
C50-2-2	0.50	4.73	9.36
C60-1-1	0.22	2.00	1.67
C60-1-2	0.22	2.00	1.67
C60-2-1	0.42	4.00	7.43
C60-2-2	0.42	4.00	7.43
CR60-1-1	0.33	3.00	3.83
CR60-1-2	0.33	3.00	3.83
Mean	0.40	3.66	5.89
Deviation coefficient	0.28	0.28	0.46

and development of new cracks. Therefore, to establish a reasonable crack width calculation formula, the effect of longitudinal tensile reinforcement on crack development should be considered in a confined concrete area. For this reason, scholars applied different perspectives by using different research methods. A method was proposed for the calculation of the effective restraint zone A_{te} of longitudinal tensile reinforcement, by considering different influencing factors. In general, A_{te} can be roughly classified in three ways: (1) as an area associated with the section depth; (2) as an area consistent with the longitudinal tensile reinforcement center of gravity; and (3) as an area related to the diameter of longitudinal tensile reinforcement d . The first two categories are convenient for practical applications. The rationality of the A_{te} value is influenced by uniformity, cross-sectional shape, and position of the tensile reinforcement. The third category corresponds to the constraint mechanism imposed by longitudinal tensile reinforcement to the surrounding concrete, which has a clear physical significance. Fig. 8 schematically shows the values of A_{te} and effective tensile depth h_{te} (discussed below) for three types of A_{te} and h_{te} provided in different specifications and approaches.

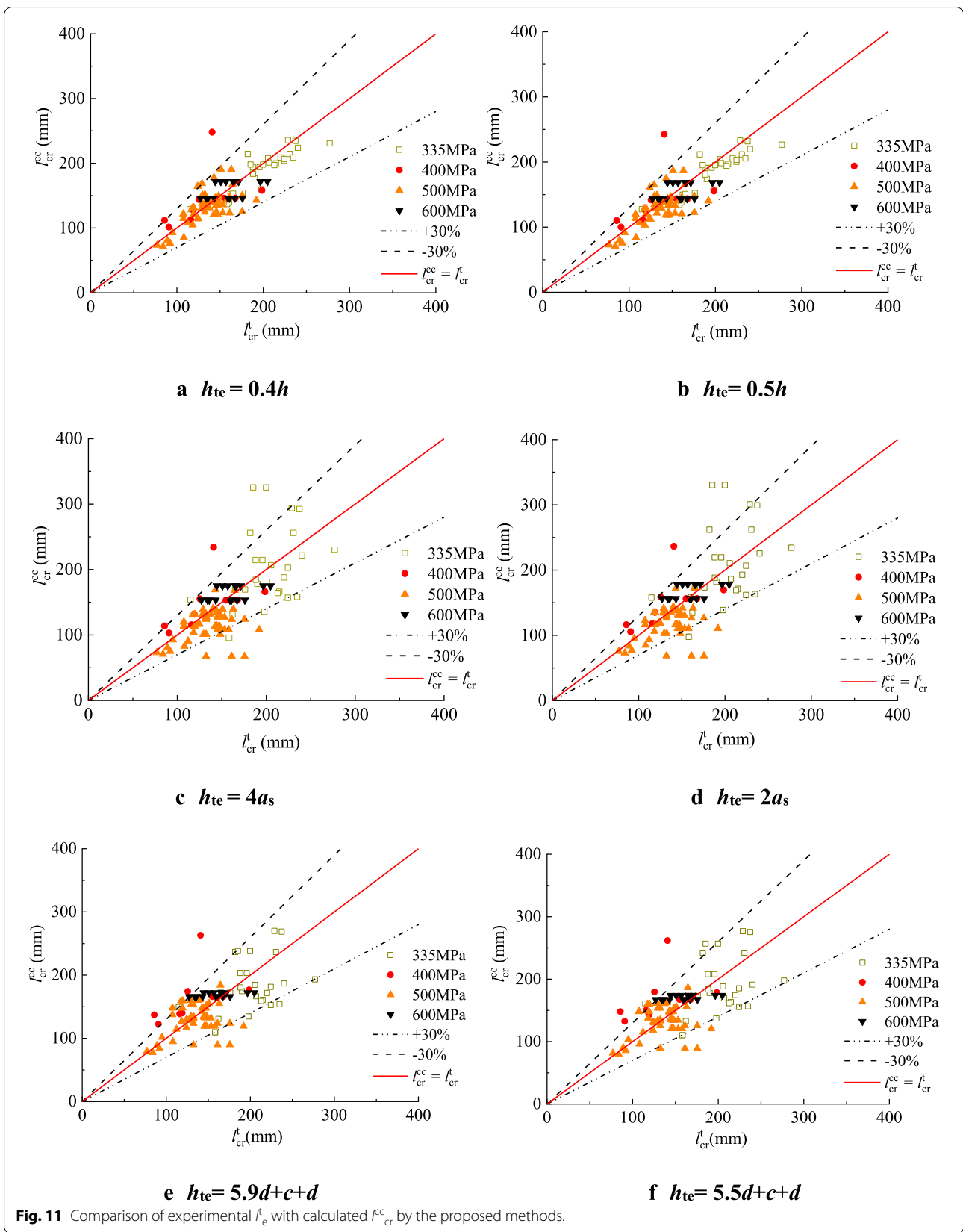


Fig. 11 Comparison of experimental f_e with calculated f_{cr}^{cc} by the proposed methods.

Table 7 Comparison of experimental f_c with calculated f_{cr}^c by the proposed methods.

Proposed methods		$h_{te}=0.4h$	$h_{te}=0.5h$	$h_{te}=4a_s$	$h_{te}=2a_s$	$h_{te}=5.9d+c+d$	$h_{te}=5.5d+c+d$
335 MPa	Mean	1.06	1.07	1.08	1.06	1.13	1.11
	Deviation coefficient	0.08	0.08	0.27	0.27	0.22	0.23
400 MPa	Mean	0.95	0.96	0.92	0.90	0.82	0.79
	Deviation coefficient	0.22	0.22	0.20	0.20	0.23	0.24
500 MPa	Mean	1.04	1.06	1.19	1.17	1.04	1.03
	Deviation coefficient	0.13	0.13	0.26	0.27	0.23	0.23
600 MPa	Mean	1.01	1.03	0.97	0.96	0.95	0.94
	Deviation coefficient	0.12	0.12	0.12	0.12	0.13	0.13
Sum	Mean	1.03	1.05	1.11	1.09	1.03	1.02
	Deviation coefficient	0.13	0.13	0.26	0.26	0.23	0.23

In this study, the effective tension-affected zone of longitudinal steel bars was experimentally determined. Widths of various cracks that formed under the normal use load level ($0.4M_u$ to $0.7M_u$) were measured at different depths of the test specimens. Typical experimentally obtained average crack widths are shown in Fig. 9, along with the depth of specimens.

Fig. 10 illustrates the proposed determination approach for the effective tensile depth h_{te} of the tested beams. By considering the test results shown in Fig. 9, the following three cases can be established to determine the effective tensile depth of a cracked section h_{te} , according to the change characteristics of a crack width and extension length range of the main crack. (1) Due to the restraint effect of the longitudinal tensile reinforcement, a crack width in the web gradually decreases after reaching its

maximum value, and the depth of the web with the maximum crack width represents the effective tensile depth of the beam h_{te} . (2) A maximum crack width appears at the beam bottom, but there is still a certain crack width at the web that does not exhibiting a linear decrease; thus, the depth corresponding to the maximum crack width at the web may be taken as the effective tensile depth of the beam h_{te} . (3) In the range of a crack extension length, a crack width decreases approximately linearly, and the actual extension depth of a crack can be considered as the effective tensile zone depth of the beam h_{te} .

Statistical analysis of cracks obtained for the loading range of $0.4M_u$ to $0.7M_u$ was conducted, and the relationships between the measured effective tensile depths for 600 MPa RC beams, h_{te}^t , and the corresponding h , a_s , and d values are shown in Table 6.

Table 8 Comparison of experimental w_{max}^t with calculated w_{max}^c by different codes and methods.

Data sources	No. of data/ <i>n</i>	ACI 318-99 (1999)		EN 1992-1-1 (2004)		GB50010 (2010)		SL/T 191-2008 (2009)		DL/T5057-2009 (2010)	
		μ	δ	μ	δ	μ	δ	μ	δ	μ	δ
335 MPa	141	1.02	0.28	0.77	0.22	0.95	0.26	0.89	0.27	0.82	0.24
400 MPa	85	0.86	0.24	0.88	0.25	0.84	0.23	1.01	0.23	0.83	0.21
500 MPa	113	0.98	0.27	1.12	0.32	1.00	0.32	1.17	0.28	0.99	0.27
600 MPa	115	1.00	0.21	0.92	0.20	0.91	0.23	0.96	0.21	0.90	0.19
Sum	454	0.98	0.24	0.91	0.30	0.92	0.26	1.00	0.27	0.89	0.25
Data sources	No. of data/ <i>n</i>	1st Zhao and Guan (2011)		JTG D62-2012 (2012)		JTJ 267-98 (1998)		TB10002.3-2005 (2005)		2nd Zhao and Guan (2010)	
		μ	δ	μ	μ	δ	δ	μ	δ	μ	δ
335 MPa	141	0.99	0.28	1.14	1.26	0.27	0.27	1.26	0.27	0.89	0.20
400 MPa	85	0.73	0.24	0.98	0.94	0.26	0.19	0.94	0.26	0.99	0.19
500 MPa	113	0.87	0.33	1.07	1.03	0.26	0.26	1.03	0.26	1.21	0.24
600 MPa	115	0.84	0.18	1.03	0.92	0.21	0.21	0.92	0.21	1.13	0.22
Sum	454	0.84	0.27	1.03	1.06	0.29	0.27	1.06	0.29	1.05	0.26

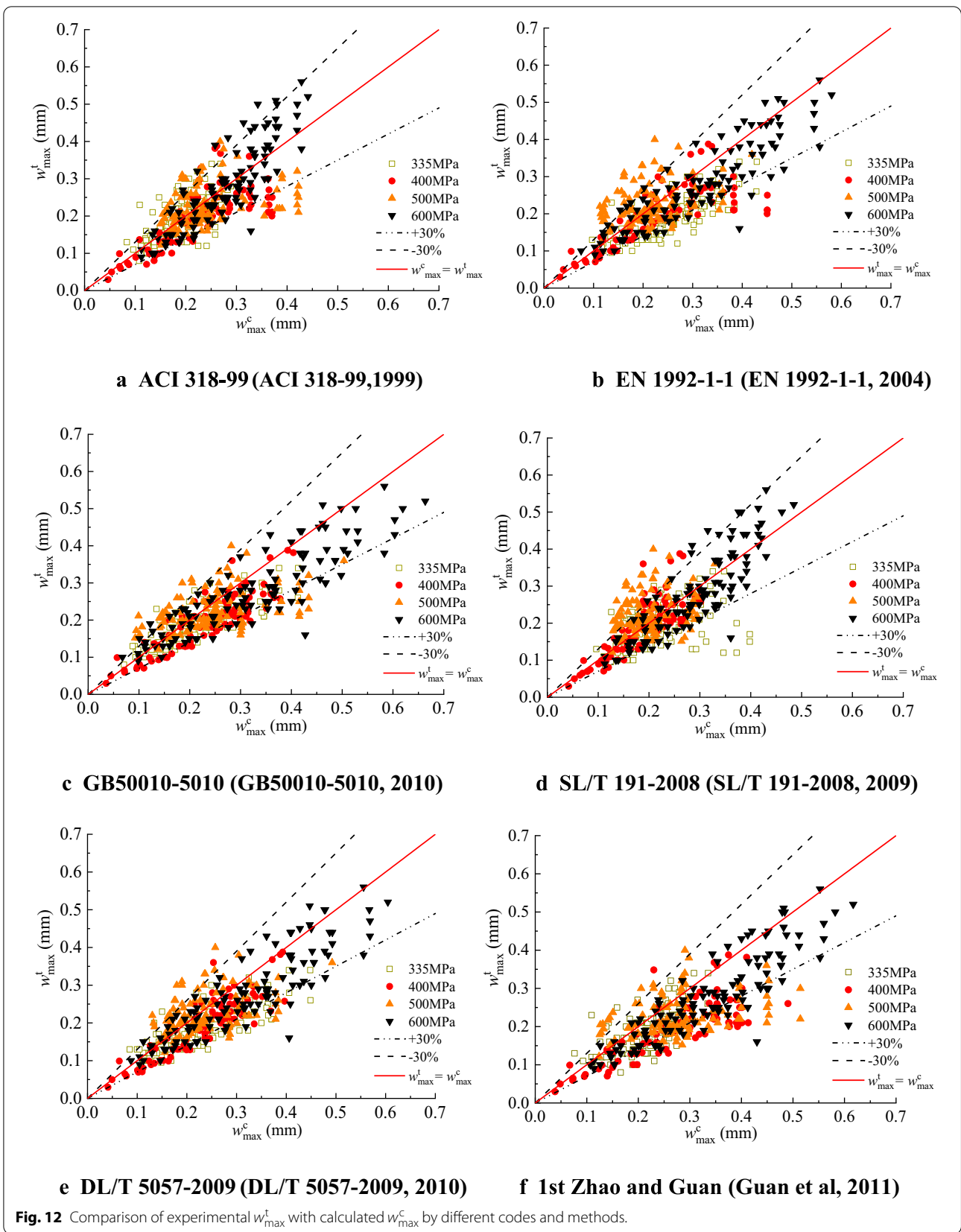
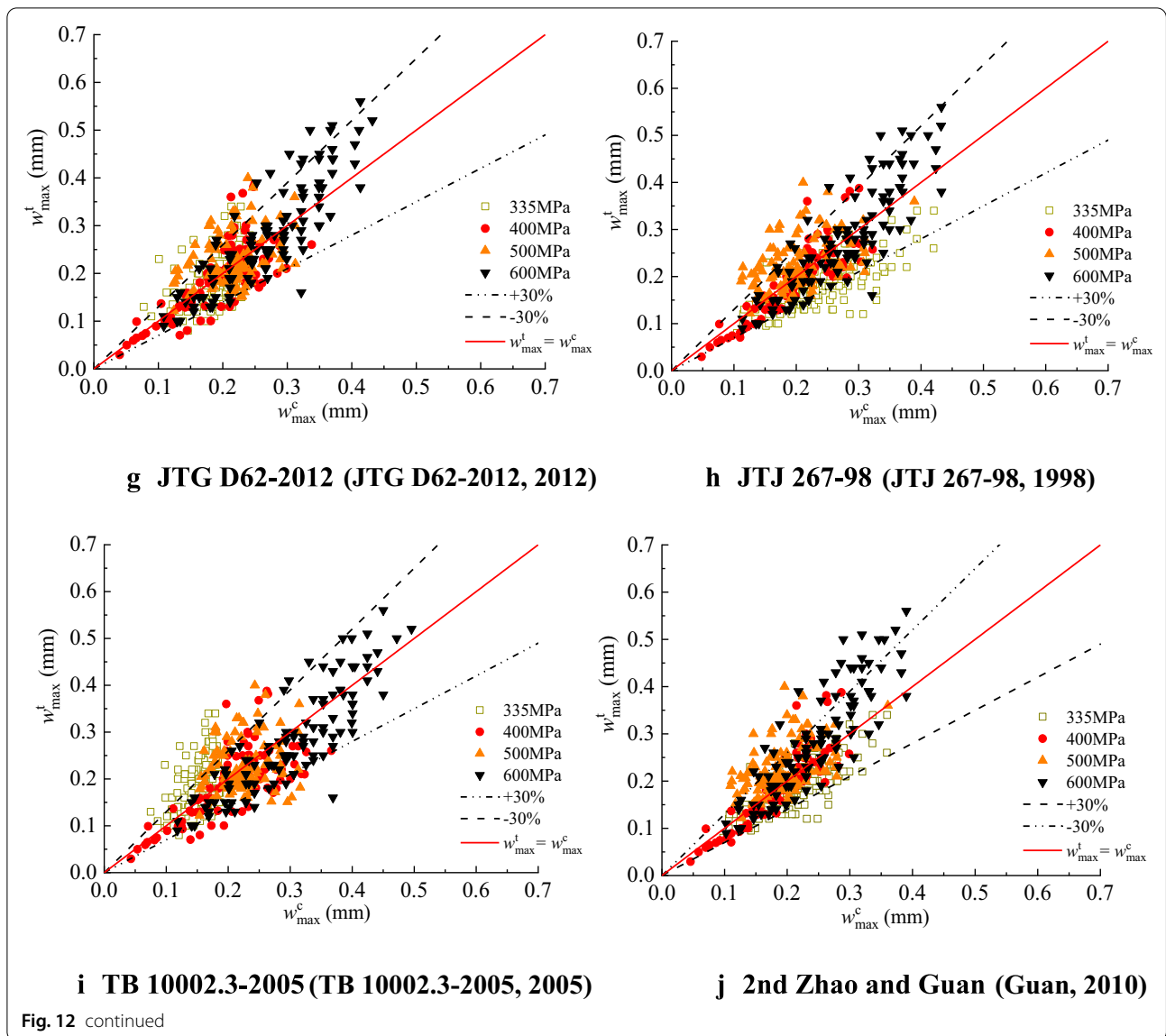


Fig. 12 Comparison of experimental w_{max}^t with calculated w_{max}^c by different codes and methods.



It can be seen from Table 6 that the relationships between h_{te}^t and h , a_s , d are $h_{te}^t = 0.4 h$; $h_{te}^t = 4a_s$; $h_{te}^t - c - d = 5.9d$, respectively. They are slightly different from the h_{te} values in the existing specifications and approaches: $h_{te} = 0.5 h$ in GB50010 (GB50010, 2010); $h_{te} = 2a_s$ in DL/T 5057, SL/T 191, JTJ 267 and TB10002.3 (DL/T 5057-1996, 1996, 2010; JTJ267-98, 1998; SL/T 191-2008, 2009; TB10002.3-2005, 2005); $h_{te} = 5.5d + a_s$ proposed by Guan et al. (2011).

It may also be mentioned that for the RC beams with 335 MPa-grade steel bars, which were experimentally examined in Guan (2010), Zhao et al. (2008, 2009), the following relations were obtained: $h_{te}^t = 0.3 h$; $h_{te}^t = 3a_s$; $h_{te}^t - c - d = 5.4d$.

4 Proposed Formulas for the Calculation of Average Crack Spacing

A comparison of formulas for the average crack spacing l_{cr} from several codes and proposals from the literature showed that c and d/ρ_{te} represent the important parameters for the determination of l_{cr} . The differences among existing formulas are the definitions of ρ_{te} and the influences of c and d/ρ_{te} . Therefore, a unified formula for l_{cr} is needed, and in this paper it is proposed as:

$$l_{cr} = k_1 c + k_2 \frac{d}{\rho_{te}}, \tag{1}$$

where k_1 and k_2 are empirical coefficients that can be determined by testing.

On the basis of the experimental results obtained in this study, three models were adopted for the determination of h_{te} . The measured values of h_{te} and the values based on the existing codes and approaches were considered in statistical analysis. Through a regression analysis of the experimental data, expressions for different average crack spacing l_{cr} were obtained as follows:

$$l_{cr} = 1.9c + 0.09 \frac{d}{\rho_{te}}, h_{te} = 0.4h \quad (2)$$

$$l_{cr} = 1.9c + 0.07 \frac{d}{\rho_{te}}, h_{te} = 0.5h \quad (2a)$$

$$l_{cr} = 1.8c + 0.09 \frac{d}{\rho_{te}}, h_{te} = 3a_s \quad (3)$$

$$l_{cr} = 1.9c + 0.18 \frac{d}{\rho_{te}}, h_{te} = 2a_s \quad (3a)$$

$$l_{cr} = 1.9c + 0.1 \frac{d}{\rho_{te}}, h_{te} = 5.9d + c + d, \text{ and } h_{te} \leq 0.5h \quad (4)$$

$$l_{cr} = 2c + 0.11 \frac{d}{\rho_{te}}, h_{te} = 5.5d + c + d, \text{ and } h_{te} \leq 0.5h \quad (4a)$$

A comparison of the experimentally determined values of average crack spacing l_{cr} , and the ones calculated from the proposed formulas (Eqs. (2) to (4)), are presented in Fig. 11 and Table 7.

As shown in Fig. 11 and Table 7, the proposed calculation model for the determination of average crack spacing l_{cr} has high precision and is suitable for the application in RC beams with 600 MPa-grade reinforcing bars. The obtained average crack spacing l_{cr} values were slightly larger than the ones obtained from existing regulations and approaches, regardless of whether the measured h_{te} values ($h_{te} = 0.4 h$; $h_{te} = 4a_s$; $h_{te} = 5.9d + c + d$) were used, or the ones based on existing formulas ($h_{te} = 0.5 h$; $h_{te} = 2a_s$; $h_{te} = 5.5d + c + d$) were applied. In general, the ratios of the measured h_{te} values to the calculated ones obtained from the depth-related method were relatively small.

5 Formulas for the Calculation of Maximum Crack Width

5.1 Assessment of the Existing Formulas and Approaches for w_{max} by Considering RC Beams with 335 to 600 MPa Steel Bars

This section summarizes the findings related to the tested beams reinforced with 335–600 MPa steel

bars. w_{max}^t corresponding to normal use-level loads is described with 454 data points. Their comparison with the w_{max}^c values calculated from the various specifications discussed above, shown in Table 8 and Fig. 12, implies that: (1) for a range of beams with 335–600 MPa-grade steel bars, only ACI 318-99 (ACI Committee, 1999) and JTG D62 (JTG D62-2012, 2012) provide acceptable results, and (2) for beams with 600 MPa-grade steel bars sufficiently accurate results can be obtained from the formulas provided in ACI 318-99 (ACI Committee, 1999), JTG D62 (JTG D62-2012, 2012) and JTJ 267 (JTJ267-98-1998, 1998).

The experimental results obtained for specimens with 600 MPa-grade reinforcing bars considered in this study, along with the experimental results for beams with 335, 400 and 500 MPa-grade bars from previous studies, were used for the analysis of applicability of the existing formulas and approaches for the maximum crack width w_{max} calculation in RC beams.

The determination of w_{max} in ACI 318-99 regulation (ACI Committee, 1999) should be conducted as:

$$w_{max} = 2 \frac{\sigma_s}{E_s} \sqrt{a_s^2 + \left(\frac{S_{max}}{2}\right)^2} \quad (5)$$

where, in addition to the previously introduced variables, σ_s is the tensile stress of steel in a cracked section and E_s denotes modulus of elasticity of steel bars.

EN1992-1-1 (2004) provides the following formula for the calculation of w_{max} :

$$w_{max} = l_{max}(\varepsilon_{sm} - \varepsilon_{cm}) \quad (6)$$

where l_{max} is the maximum crack spacing, $\varepsilon_{sm} - \varepsilon_{cm} = [\sigma_s - k_t f_t (1 + \alpha_e \rho_{te}) / \rho_{te}] / E_s \geq 0.6 \sigma_s / E_s$, k_t is the coefficient that depends on load duration (for short- and long-term loads k_t amounts to 0.6 and 0.4, respectively), and α_e is the ratio of the elastic moduli of reinforcing steel and concrete.

The calculation formula for w_{max} under short-term loads provided in GB50010 (2010) reads:

$$w_{max} = 0.85 \tau_s \psi \frac{\sigma_s}{E_s} \left(1.9c + 0.08 \frac{d}{\rho_{te}} \right) \quad (7)$$

where τ_s represents the expansion coefficient of crack width, with the value of 1.66 for RC flexural concrete members, and ψ is the strain non-uniformity coefficient of tensile steel bars between cracks. ψ is defined as $1.1 - 0.65 f_{tk} / (\rho_{te} \sigma_s)$, where σ_s denotes tensile stress of steel in a cracked section and it is equal to $M / (0.87 A_s h_0)$, with $\rho_{te} = A_s / (h_{te} b)$ and $h_{te} = 0.5 h$.

According to SL/T 191-2008 (2009), under short-term loads w_{max} can be determined as:

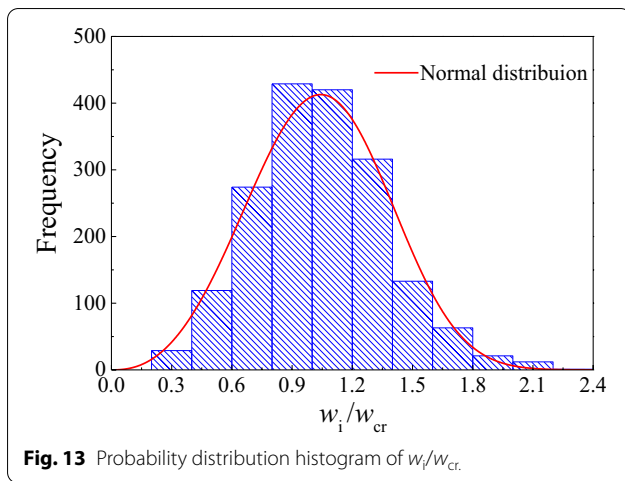


Fig. 13 Probability distribution histogram of w_i/w_{cr} .

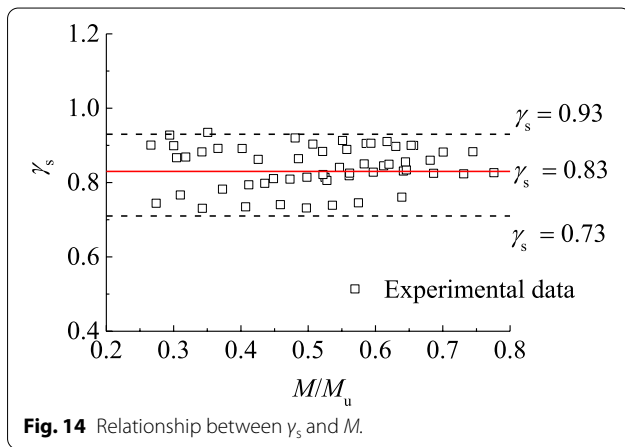


Fig. 14 Relationship between γ_s and M .

$$w_{max} = 1.4 \frac{\sigma_s}{E_s} \left(30 + c + 0.07 \frac{d}{\rho_{te}} \right) \tag{8}$$

for $\rho_{te} = A_s / (h_{te} b)$, $h_{te} = 2a_s$.

Under short-term loads, based on DL/T 5057-2009 (2010), w_{max} should be calculated as:

$$w_{max} = 1.27 \psi \frac{\sigma_s}{E_s} \left(2.2c + 0.09 \frac{d}{\rho_{te}} \right) \tag{9}$$

for $\psi = 1 - 1.1f_{tk} / (\rho_{te} \sigma_s)$ and $h_{te} = 2a_s$.

Calculation formula for w_{max} , applicable to large-size RC members with large concrete cover, was proposed by Guan et al. (2011):

$$w_{max} = 1.6 \frac{0.7}{0.875 + 0.00025h} \frac{\sigma_s}{E_s} \left(1 - \frac{0.5f_t}{\rho_{te}\sigma_s} \right) \left(1.9c + 0.014 \frac{d}{\rho_{te}} \frac{h}{a_s} \right) \tag{10}$$

where $h_{te} = 5.5d + a_s$ applies for a single row of steel bars and $h_{te} = 5.5d + s + a_s$ applies for two rows of steel bars, as shown in Fig. 8c.

Formula for w_{max} under short-term loads based on JTJ D62 provisions (JTJ D62-2012, 2012) reads:

$$w_{max} = C_1 C_2 \frac{\sigma_s}{E_s} \left(\frac{30 + d}{0.28 + 10\rho} \right) \tag{11}$$

where C_1 is the surface shape coefficient of reinforcing bars and C_2 denotes the coefficient related to the mechanical properties of a member.

According to JTJ 267 (1998), under short-term loads w_{max} can be obtained as:

$$w_{max} = C_1 C_2 \frac{\sigma_s}{E_s} \left(\frac{c + d}{0.3 + 1.4\rho_{te}} \right) \tag{12}$$

for $h_{te} = 2a_s$.

TB10002.3 (2005) provides the following expression for the determination of w_{max} under short-term loads:

$$w_{max} = K_1 K_2 \gamma \frac{\sigma_s}{E_s} \left(80 + \frac{8 + 0.4d}{\sqrt{\rho_{te}}} \right) \tag{13}$$

where K_1 depends on bar surface shape ($K_1 = 0.8$ for ribbed bars), and K_2 depends on load characteristics. K_2 is defined as $(1 + \alpha M_1 / M + 0.5 M_2 / M)$, where $\alpha = 0.3$ for ribbed bars, M_1 is the bending moment under live load action, M_2 is the bending moment under constant load action and M is the bending moment under the action of all loads. Furthermore, γ is the ratio of a distance between the neutral axis and concrete face and a distance between the neutral axis and center of gravity of reinforced bars (for beams it is equal to 1.1). For Eq. (13), $h_{te} = 2a_s$ applies.

The calculation formula for w_{max} , applicable to large-size RC members with large concrete cover, was proposed by Guan et al. (2010):

$$w_{max} = \frac{\sigma_s}{E_s} \left(\frac{0.76c + d}{0.3 + 1.4\rho_{te}} \right) \tag{14}$$

where h_{te} is introduced above.

Equations (5) to (10) are semi-theoretical and semi-empirical. The following formulas, i.e., Eqs. (11) to (14), can be considered as statistical ones. Accordingly, the sub-figures (a)~(f) in Fig. 12 are the comparative analysis results of calculated values and measured values based on semi-theoretical and semi-empirical modes. In Fig. 12, the sub-figures (g)~(j) are the comparative analysis results of calculated and measured values based on a mathematical statistics model.

From Table 8 and Fig. 12, it can be deduced that: (1) for the beams with 335–600 MPa-grade steel bars, only ACI

318-99 (ACI Committee, 1999) and JTG D62 (JTGD62-2012, 2012) hold good and provide satisfactory results, and (2) for beams with 600 MPa-grade steel bars sufficiently accurate results can be obtained from the formulas provided in ACI 318-99 (ACI Committee, 1999), JTG D62 (JTG D62-2012, 2012) and JTJ 267 (JTJ267-98, 1998).

5.2 Based on Semi-Theoretical and Semi-Empirical Calculation Model

On the basis of the bond slip theory, a formula for the determination of the maximum crack width w_{max} in RC beams presented in Zang (2007) reads:

$$w_{max} = \tau_s \alpha_c \frac{\sigma_s}{E_s} \psi l_{cr} \tag{15}$$

where, in addition to the previously defined variables, τ_s (also defined above) can be determined based on the probability distribution of measured crack widths, and α_c is the comprehensive coefficient which takes into account the influences of tensile and shrinkage concrete deformation and cross-sectional shape, and can be determined by testing. Equation (15) is considered to be semi-theoretical and semi-empirical.

To obtain an accurate guarantee rate of the crack width, the ratios of measured widths w_i to mean widths w_{cr} (w_i/w_{cr}) were used to create a probability distribution histogram shown in Fig. 13. Statistical analysis of 20,000 crack width data obtained in this experiment showed that the w_i/w_{cr} ratio basically conformed to a normal distribution. The mean value was $\mu = 1$, and the mean square deviation was $\sigma = 0.344$ corresponding to the 95% guarantee rate. $\tau_s = \mu + 1.645\sigma = 1.612$, and $\sigma = 1.61$. In this study, τ_s was 1.6.

The formula for the calculation of reinforcement stress in cracked cross sections provided in GB50010 (2010), SL/T 191 (2009), DL/T 5057 (2010), JTG D62-2012 (2012), JTJ 267 (1998), and TB10002.3 (2005) codes reads:

$$\sigma_s = \frac{M}{A_s \gamma_s h_0} \tag{16}$$

where M refers to the measured bending moment of the specimen, γ_s denotes the internal lever arm coefficient in a cracked section, and on the basis of the above listed Chinese regulations it is equal to 0.8.

In this experiment, strain gauges were attached to the longitudinal reinforcing bars to capture the stress change in cracked sections. The corresponding measured internal lever arm coefficient γ_s was determined as $M/(\sigma_s A_s h_0)$, based on the calculation model of measured and standard reinforcement stresses. The change of its measured

value with the bending moment is shown in Fig. 14. The maximum and minimum measured values were 0.93 and 0.73 (respectively), producing an average of 0.83.

A detailed comparison of the results indicated small differences related to the calculation of ψ in GB50010 (2010), SL/T 191 (SL & T, 2009) and DL/T 5057 (DL & T, 2010). Thus, for convenience, the GB50010 (2010) formula was adopted in this study, i.e., $\psi = 1.1 - 0.65f_t/(\rho_{te}\sigma_s)$.

w_{max} is obtained by using Eqs. (2) and (15), and $\alpha_c = 0.71$ and $\tau_s = 1.61$ determined from the regression analysis:

$$w_{max} = 1.61 \times 0.71 \times \frac{M}{0.83E_s A_s h_0} \times \left(1.1 - 0.65 \frac{f_t}{\rho_{te}\sigma_s}\right) \times \left(1.9c + 0.09 \frac{d}{\rho_{te}}\right) \tag{17}$$

w_{max} is obtained by using Eqs. (2a) and (15), and $\alpha_c = 0.82$ and $\tau_s = 1.61$ determined from the regression analysis:

$$w_{max} = 1.61 \times 0.82 \times \frac{M}{0.83E_s A_s h_0} \times \left(1.1 - 0.65 \frac{f_t}{\rho_{te}\sigma_s}\right) \times \left(1.9c + 0.07 \frac{d}{\rho_{te}}\right) \tag{18}$$

w_{max} is obtained by using Eqs. (3) and (15), and $\alpha_c = 0.72$ and $\tau_s = 1.61$ determined from the regression analysis:

$$w_{max} = 1.61 \times 0.72 \times \frac{M}{0.83E_s A_s h_0} \times \left(1.1 - 0.65 \frac{f_t}{\rho_{te}\sigma_s}\right) \times \left(1.8c + 0.09 \frac{d}{\rho_{te}}\right) \tag{19}$$

w_{max} is obtained by using Eqs. (3a) and (15), and $\alpha_c = 0.58$ and $\tau_s = 1.61$ determined from the regression analysis:

$$w_{max} = 1.61 \times 0.58 \times \frac{M}{0.83E_s A_s h_0} \times \left(1.1 - 0.65 \frac{f_t}{\rho_{te}\sigma_s}\right) \times \left(1.9c + 0.18 \frac{d}{\rho_{te}}\right) \tag{20}$$

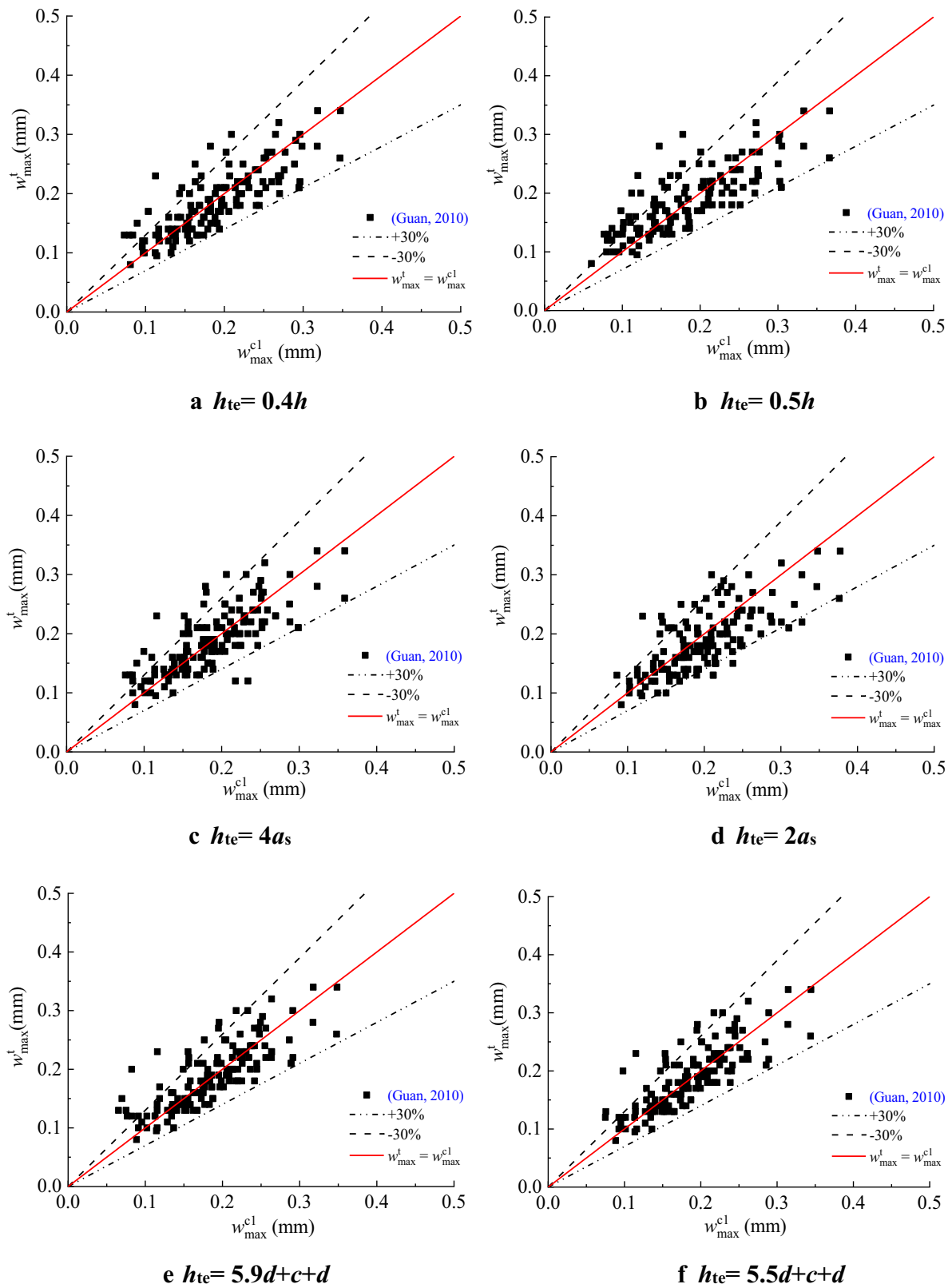


Fig. 15 Comparison of experimental w_{max}^t from RC beams with 335 MPa steel bars with calculated w_{max}^{c1} by the proposed methods.

Table 9 Comparison results of w_{max}^t from RC beams with 335 MPa steel bars with w_{max}^{c1} by the proposed methods.

Data sources	No.of data /n	$h_{te}=0.4h$		$h_{te}=0.5h$		$h_{te}=4a_s$		$h_{te}=2a_s$		$h_{te}=5.9d+c+d$		$h_{te}=5.5d+c+d$	
		μ	δ	μ	δ	μ	δ	μ	δ	μ	δ	μ	δ
Guan (2010)	141	1.02	0.22	1.08	0.24	1.04	0.22	0.96	0.23	1.05	0.25	1.03	0.21

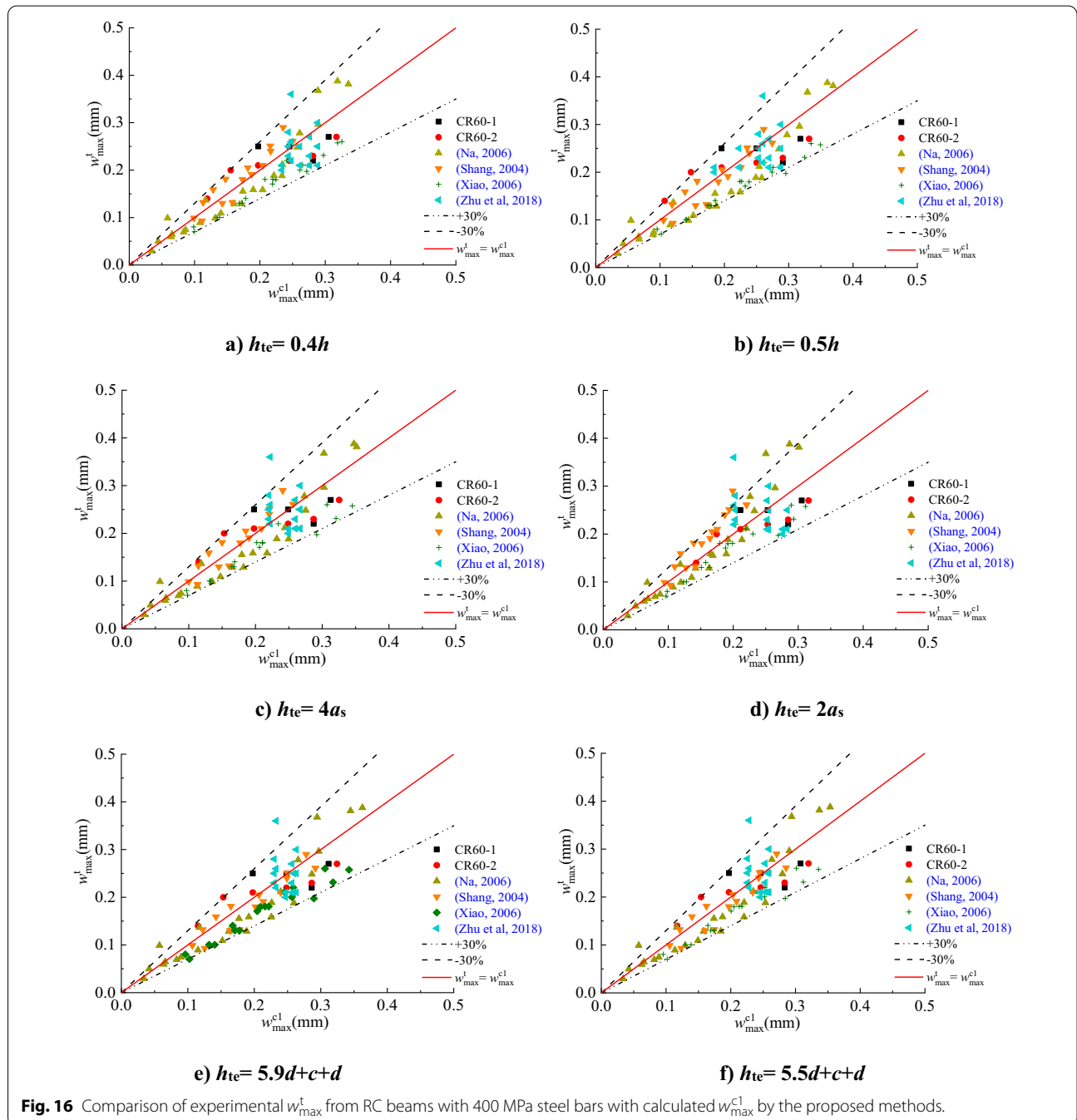


Fig. 16 Comparison of experimental w_{max}^t from RC beams with 400 MPa steel bars with calculated w_{max}^{c1} by the proposed methods.

Table 10 Comparison results of w_{max}^t from RC beams with 400 MPa steel bars with w_{max}^{c1} by the proposed methods.

Data sources	No. of data/n	$h_{te}=0.4h$		$h_{te}=0.5h$		$h_{te}=4a_s$		$h_{te}=2a_s$		$h_{te}=5.9d+c+d$		$h_{te}=5.5d+c+d$	
		μ	δ	μ	δ	μ	δ	μ	δ	μ	δ	μ	δ
CR60-1-1	4	0.99	0.21	0.97	0.24	0.97	0.22	0.96	0.18	0.98	0.22	0.98	0.22
CR60-1-2	6	1.01	0.19	1.04	0.24	1.02	0.21	0.94	0.13	1.02	0.21	1.02	0.20
Na (2006)	25	0.96	0.22	0.90	0.26	0.94	0.24	1.01	0.20	0.94	0.24	0.95	0.23
Shang (2004)	15	1.07	0.12	0.98	0.13	1.05	0.12	1.18	0.13	0.94	0.13	0.96	0.13
Xiao (2006)	19	0.79	0.06	0.75	0.06	0.81	0.08	0.87	0.10	0.79	0.08	0.80	0.08
Zhu et al. (2018)	16	0.95	0.18	0.99	0.16	1.01	0.22	1.05	0.27	1.00	0.20	1.02	0.20
Sum	85	0.94	0.20	0.91	0.22	0.95	0.21	1.01	0.21	0.92	0.20	0.94	0.20

w_{max} is obtained by using Eqs. (4) and (15), and $\alpha_c=0.66$ and $\tau_s = 1.61$ determined from the regression analysis:

$$w_{max} = 1.61 \times 0.66 \times \frac{M}{0.83E_sA_s h_0} \times \left(1.1 - 0.65 \frac{f_t}{\rho_{te}\sigma_s}\right) \times \left(1.9c + 0.1 \frac{d}{\rho_{te}}\right) \tag{21}$$

w_{max} is obtained by using Eqs. (4a) and (15), and $\alpha_c=0.66$ and $\tau_s = 1.61$ determined from the regression analysis:

$$w_{max} = 1.61 \times 0.61 \times \frac{M}{0.83E_sA_s h_0} \times \left(1.1 - 0.65 \frac{f_t}{\rho_{te}\sigma_s}\right) \times \left(2c + 0.11 \frac{d}{\rho_{te}}\right) \tag{22}$$

5.2.1 Assessment of the Method for RC Beams with Steel Bars of Various Yield Strengths

(1) Beams with 335 MPa-Grade Steel Bars

For RC beams with 335 MPa steel bars, a comparison between maximum crack widths w_{max}^t obtained from the tests under serviceability-level loads and the w_{max}^{c1} values calculated by using the proposed method is shown in Fig. 15 and Table 9. The results indicate that the proposed method leads to a good estimation of maximum crack widths in the case of RC beams with 335 MPa steel bars.

(2) Beams with 400 MPa-Grade Steel Bars

For RC beams with 400 MPa steel bars, a comparison between maximum crack widths w_{max}^t obtained from the tests under serviceability-level loads and the w_{max}^{c1} values calculated by using the proposed method is shown in Fig. 16 and Table 10. The results indicate that the proposed method leads to a good estimation of maximum crack widths in the case of RC beams with 400 MPa steel bars.

Table 11 Comparison results of w_{max}^t from RC beams with 500 MPa steel bars with w_{max}^{c1} by the proposed methods.

Data sources	No. of data/n	$h_{te}=0.4h$		$h_{te}=0.5h$		$h_{te}=4a_s$		$h_{te}=2a_s$		$h_{te}=5.9d+c+d$		$h_{te}=5.5d+c+d$	
		μ	δ	μ	δ	μ	δ	μ	δ	μ	δ	μ	δ
Zhu et al. (2018)	16	0.75	0.16	0.75	0.21	0.81	0.16	0.86	0.19	0.80	0.15	0.82	0.15
Wang et al. (2007)	5	0.77	0.14	0.72	0.12	0.87	0.13	0.99	0.17	0.84	0.12	0.86	0.12
Zhang (2004)	18	1.01	0.14	1.01	0.16	1.06	0.13	1.12	0.17	1.01	0.12	1.03	0.12
Xu (2007)	30	1.26	0.21	1.32	0.31	1.21	0.22	1.23	0.29	1.20	0.24	1.22	0.25
Dang (2009)	9	1.09	0.15	1.09	0.22	1.29	0.21	1.34	0.19	1.14	0.21	1.16	0.21
Wang (2007)	9	1.33	0.20	1.23	0.21	1.38	0.21	1.45	0.19	1.26	0.24	1.29	0.24
Li (2007)	7	1.26	0.10	1.17	0.10	1.26	0.10	1.31	0.11	1.22	0.11	1.24	0.11
Liu (2012)	12	0.81	0.19	0.75	0.18	0.82	0.17	0.93	0.18	0.81	0.15	0.83	0.15
Zang (2007)	7	1.62	0.10	1.54	0.10	1.69	0.10	1.70	0.10	1.57	0.13	1.60	0.12
Sum	113	1.09	0.29	1.08	0.33	1.13	0.28	1.14	0.28	1.08	0.27	1.10	0.27

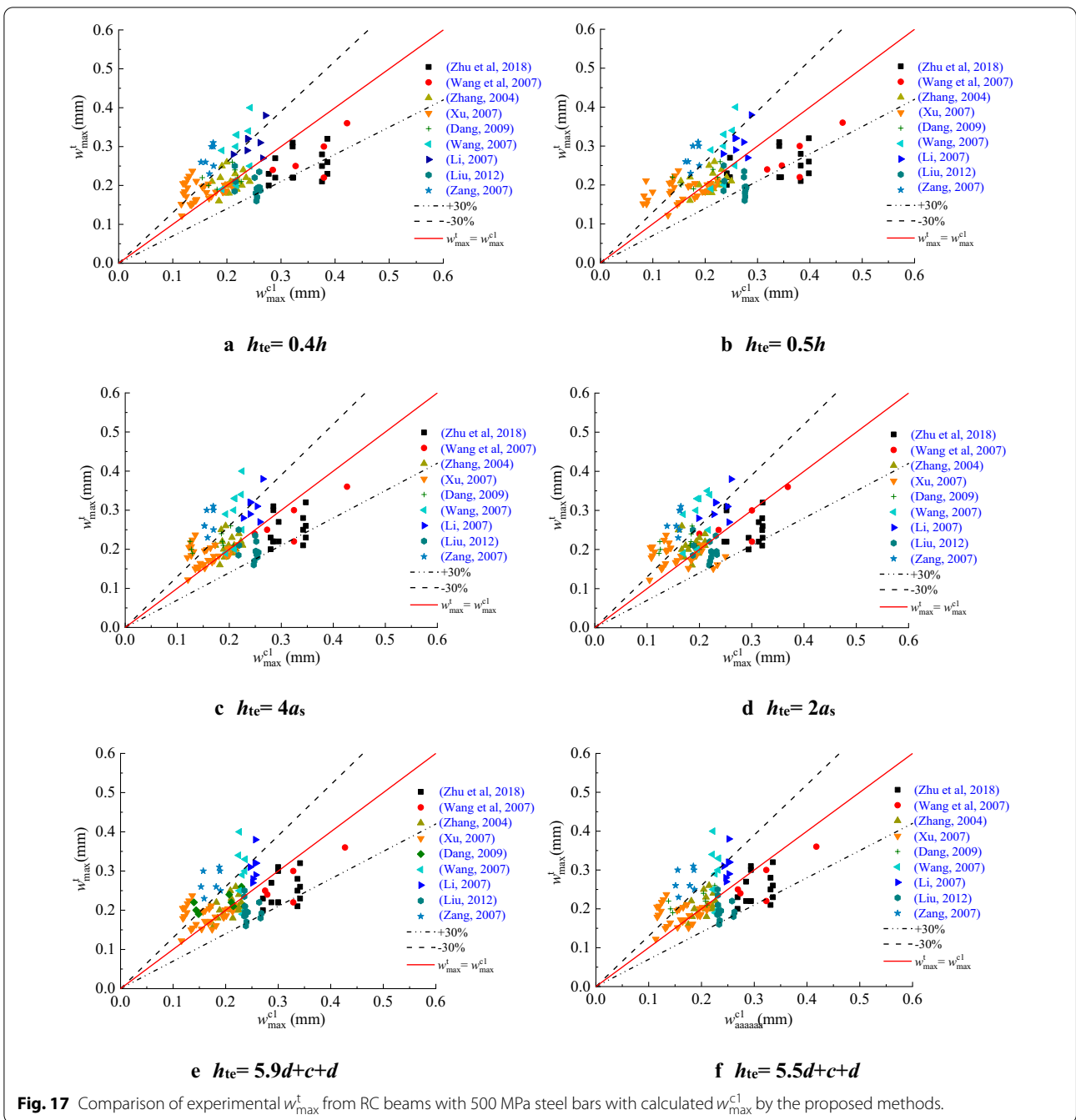


Table 12 Comparison results of w_{max}^t from RC beams with 600 MPa steel bars with w_{max}^{c1} by the proposed methods.

Data sources	No. of data /n	$h_{te}=0.4h$		$h_{te}=0.5h$		$h_{te}=4a_s$		$h_{te}=2a_s$		$h_{te}=5.9d+c+d$		$h_{te}=5.5d+c+d$	
		μ	δ	μ	δ	μ	δ	μ	δ	μ	δ	μ	δ
C30-1-1	7	0.80	0.08	0.77	0.13	0.78	0.10	0.80	0.05	0.78	0.10	0.79	0.09
C30-1-2	7	1.16	0.08	1.11	0.09	1.13	0.08	1.16	0.11	1.13	0.08	1.15	0.08
C30-2-1	4	0.80	0.07	0.79	0.12	0.79	0.08	0.79	0.02	0.82	0.05	0.83	0.05
C30-2-2	6	1.22	0.07	1.25	0.09	1.22	0.07	1.15	0.11	1.24	0.07	1.26	0.08
C40-1-1	9	1.01	0.16	0.99	0.23	0.99	0.19	0.99	0.09	0.99	0.19	1.00	0.17
C40-1-2	10	0.88	0.07	0.86	0.11	0.86	0.08	0.87	0.07	0.87	0.08	0.88	0.07
C40-2-1	7	0.98	0.12	0.99	0.16	0.97	0.13	0.93	0.07	1.00	0.10	1.01	0.10
C40-2-2	7	0.86	0.07	0.87	0.09	0.86	0.07	0.85	0.13	0.88	0.09	0.89	0.10
C50-1-1	10	0.86	0.23	0.83	0.22	0.85	0.22	0.87	0.25	0.85	0.22	0.86	0.23
C50-1-2	10	1.07	0.08	1.06	0.10	1.06	0.08	1.05	0.12	1.06	0.08	1.07	0.08
C50-2-1	5	1.20	0.04	1.25	0.06	1.20	0.04	1.10	0.05	1.22	0.04	1.22	0.04
C50-2-2	7	1.02	0.09	1.12	0.18	1.03	0.10	0.90	0.08	1.02	0.07	1.02	0.07
C60-1-1	8	1.06	0.13	1.03	0.17	1.04	0.15	1.03	0.09	1.04	0.15	1.05	0.14
C60-1-2	7	0.87	0.17	0.93	0.29	0.89	0.22	0.80	0.06	0.89	0.21	0.88	0.19
C60-2-1	6	0.86	0.13	0.96	0.22	0.87	0.14	0.74	0.04	0.86	0.10	0.86	0.09
C60-2-2	5	0.88	0.14	0.95	0.20	0.89	0.15	0.79	0.10	0.89	0.13	0.89	0.12
Sum	115	0.97	0.17	0.98	0.21	0.96	0.18	0.93	0.17	0.97	0.18	0.98	0.17

Table 13 Comparison results of w_{max}^t from RC beams with 335 MPa–600 MPa steel bars with w_{max}^{c1} by the proposed methods.

Data sources	No. of data /n	$h_{te}=0.4h$		$h_{te}=0.5h$		$h_{te}=4a_s$		$h_{te}=2a_s$		$h_{te}=5.9d+c+d$		$h_{te}=5.5d+c+d$	
		μ	δ	μ	δ	μ	δ	μ	δ	μ	δ	μ	δ
335 MPa	141	1.02	0.22	1.08	0.24	1.04	0.22	0.96	0.23	1.05	0.25	1.03	0.21
400 MPa	85	0.94	0.20	0.91	0.22	0.95	0.21	1.01	0.21	0.92	0.20	0.94	0.20
500 MPa	113	1.09	0.29	1.08	0.33	1.13	0.28	1.18	0.28	1.08	0.27	1.10	0.27
600 MPa	115	0.97	0.17	0.98	0.21	0.96	0.18	0.93	0.17	0.97	0.18	0.98	0.17
Sum	454	1.01	0.23	1.02	0.27	1.02	0.24	1.02	0.25	1.01	0.24	1.02	0.23

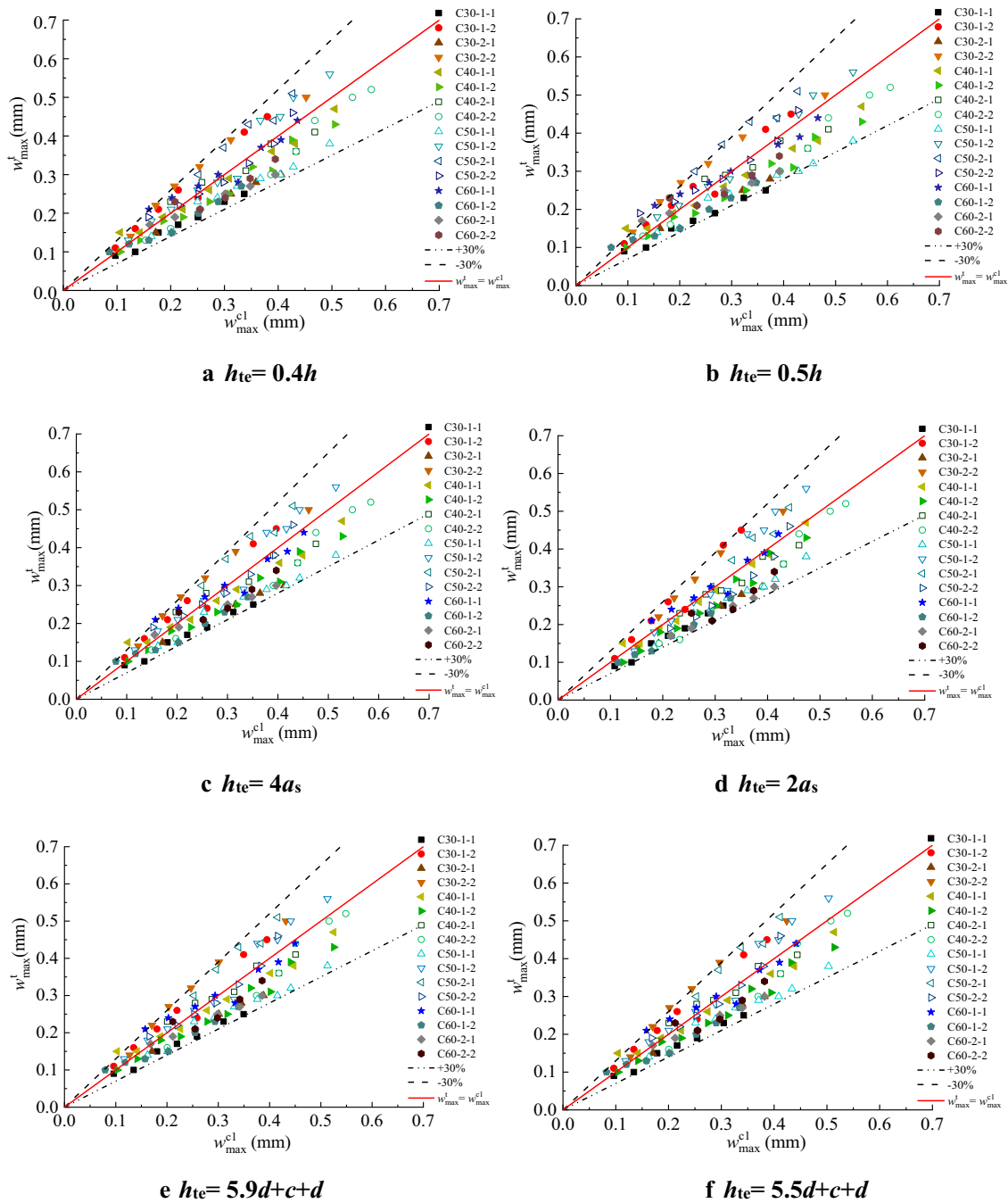
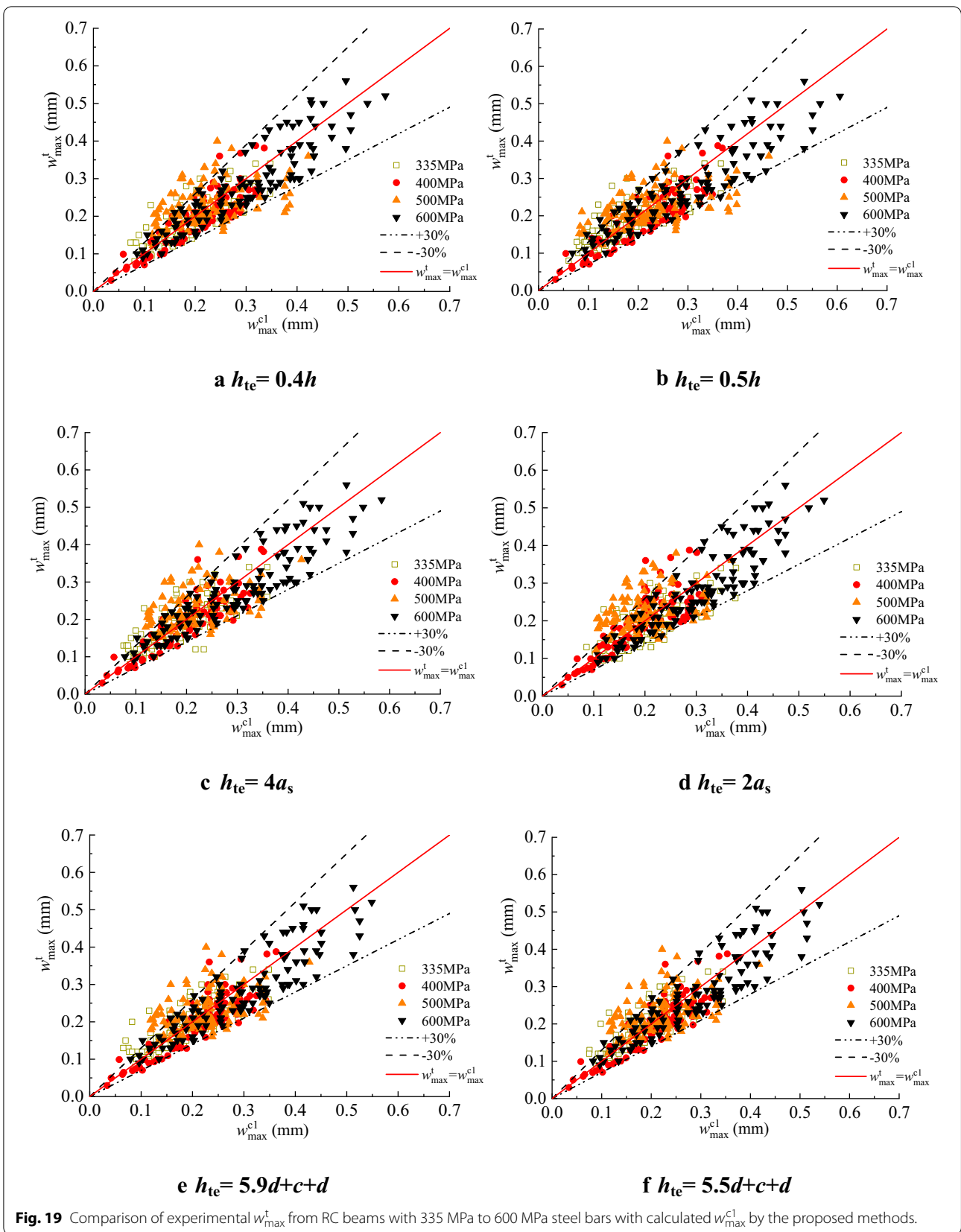


Fig. 18 Comparison of experimental w_{max}^t from RC beams with 600 MPa steel bars with calculated w_{max}^{c1} by the proposed methods.



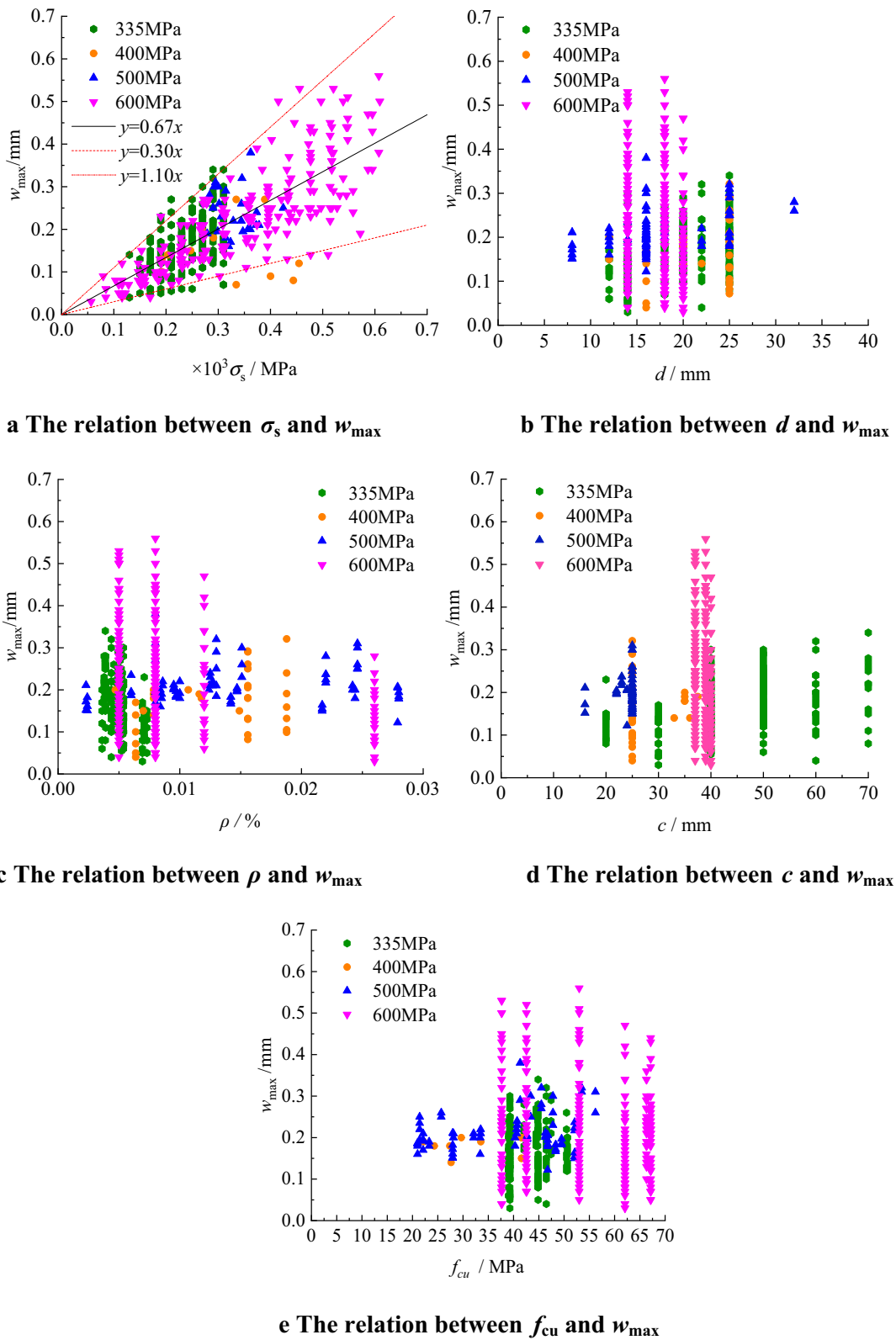


Fig. 20 Comparison of w_{max} and different parameters such as σ_s , d , ρ , c , f_{cu} from RC beams with 335 MPa–600 MPa steel bars.

(3) Beams with 500 MPa-Grade Steel Bars

For RC beams with 500 MPa steel bars, a comparison between maximum crack widths w_{\max}^t obtained from the tests under serviceability-level loads and the w_{\max}^{cl} values calculated by using the proposed method is shown in Fig. 17 and Table 11. The results indicate that the proposed method leads to a good estimation of maximum crack widths in the case of RC beams with 500 MPa steel bars.

(4) Beams with 600 MPa-Grade steel Bars

For RC beams with 600 MPa steel bars, a comparison between maximum crack widths w_{\max}^t obtained from the tests under serviceability-level loads and the w_{\max}^{cl} values calculated by using the proposed method is shown in Fig. 18 and Table 12. The results indicate that the proposed method leads to a good estimation of maximum crack widths in the case of RC beams with 600 MPa steel bars.

(5) Beams with 335 to 600 MPa-Grade Steel Bars

For RC beams with 335 to 600 MPa steel bars, a comparison between maximum crack widths w_{\max}^t obtained from the tests under serviceability-level loads and the w_{\max}^{cl} values calculated by using the method is shown in Fig. 19 and Table 13. The results indicate that the method leads to a good estimation of maximum crack widths in the case of RC beams with 335 to 600 MPa steel bars. Additionally, the accuracy results for beams with 500–600 MPa steel bar is improved compared to the existing approaches.

6 A Unified Formula for the Calculation of Maximum Crack Width for RC Beams with 335–600 MPa-Grade Steel Bars

From the analysis presented and discussed above, it can be seen that the parameters for the calculation of maximum crack width are complex and inconvenient to use. According to different codes, a maximum crack width of an RC beam is related to: longitudinal reinforcement stress, reinforcement diameter, longitudinal reinforcement ratio, concrete cover and concrete strength. Based on a large number of experimental data for RC beams with 335–600 MPa steel bars, the obtained relationships are presented in Fig. 20. A comparison shows that the longitudinal reinforcement stress provides sufficient accuracy when calculating the maximum crack width for RC beams with 335–600 MPa steel bars. The most influential factor on the maximum crack width of reinforced concrete beams is the longitudinal reinforcement stress, which has a particular linear relationship with the maximum crack width (Fig. 20a). However, the influence of reinforcement diameter, longitudinal reinforcement ratio, protective layer thickness and concrete

strength on the maximum crack width was not noticeable. The data scatter was relatively large (Fig. 20b–e). The longitudinal reinforcement stress was selected as the main parameter, and the regression analysis was carried out using mathematical statistics method. The expression between the longitudinal reinforcement stress and the maximum crack width w_{\max} is $y=0.67x$, and the test data points are mainly distributed between the straight lines $y=0.30x$ and $y=1.10x$ in Fig. 20 a). The developed unified expression is useful as it provides a reference and guiding tool for different engineering applications.

7 Conclusions

The occurrence and development of cracks and their width variation were determined experimentally under various load levels. The obtained test results were used for the establishment of calculation models for the determination of crack spacing and width applicable to beams with 335–600 MPa. The main conclusions are provided below.

1. Statistical analysis of the cracks developed in beams (reinforced with 600 MPa steel bars) under pure bending indicated a continuous extension of cracks under different loads after an initial cracking, or their rapid progression toward the neutral axis.

2. The following relationships were established for RC beams with 600 MPa and 400 MPa steel bars corresponding to normal load levels, respectively: $h_{te}^t=0.4 h$, $h_{te}^t=4a_s$, and $h_{te}^t=5.9d$.

3. The measured values of average crack spacing obtained in this study differed from the values determined from other codes. The ratios between the calculated and measured values of maximum crack widths were relatively large.

4. An expression for the calculation of average crack spacing in concrete beams with steel bars of various yield strengths (335 to 600 MPa) has been proposed in this paper. Also, expressions for the calculation of the maximum crack width have been developed.

5. A unified formula with RC beams with 335–600 MPa-grade steel bars to calculate maximum crack width has been proposed. The application of longitudinal reinforcement stress provided sufficient accuracy of the calculated maximum crack widths in RC beams with 335–600 MPa-grade steel bars.

Acknowledgements

Not applicable.

Authors' contributions

XY and JG designed the experiments. LZ and JX carried out the experiments. XY, JG and LL analyzed the experimental results. XY and JG reviewed and edited the manuscript. JG received the funding. All authors read and approved the final manuscript.

Authors' information

Xianhua Yao is lecturer in School of Civil Engineering and Communication, North China University of Water Resources and Electric Power, Zhengzhou 450045, Henan, China.

Junfeng Guan is Professor in School of Civil Engineering and Communication, North China University of Water Resources and Electric Power, Zhengzhou 450045, Henan, China.

Lei Zhang is Senior Engineer in Institute of Engineering Mechanics, Yellow River Institute of Hydraulic Research, Zhengzhou 450099, Henan, China.

Junyi Xi is Postgraduate student in School of Civil Engineering and Communication, North China University of Water Resources and Electric Power, Zhengzhou 450045, Henan, China.

Lielie Li is lecturer in School of Civil Engineering and Communication, North China University of Water Resources and Electric Power, Zhengzhou 450045, Henan, China.

Funding

This project was sponsored by the National Natural Science Foundation of China (51779095, 52179132), Program for Science and Technology Innovation Talents in Universities of Henan Province (20HASTIT013), Sichuan Univ, State Key Lab Hydraul and Mt River Engr (SKHL2007).

Availability of data and materials

The datasets used and/or analyzed during the current study are available from the corresponding author on reasonable request.

Declarations

Competing interests

The authors declare no conflicts of interest to this work.

Author details

¹School of Civil Engineering and Communication, North China University of Water Resources and Electric Power, Zhengzhou 450045, Henan, China.

²Institute of Engineering Mechanics, Yellow River Institute of Hydraulic Research, Zhengzhou 450099, Henan, China.

Received: 22 July 2021 Accepted: 2 October 2021

Published online: 22 October 2021

References

- ACI Committee 318. (1971). *Building code requirement for structural concrete (ACI 318-71)*. American Concrete Institute.
- ACI Committee 318. (1995). *Building code requirement for structural concrete (ACI 318-95) and commentary (ACI 318R-95)*. American Concrete Institute.
- ACI Committee 318. (1999). *Building code requirement for structural concrete (ACI 318-99) and commentary (ACI 318R-99)*. American Concrete Institute.
- ACI Committee 318. (2014). *Building code requirement for structural concrete (ACI 318-14) and commentary (ACI 318R-14)*. American Concrete Institute.
- ASTM A706/A706M-14. (2014). *Standard specification for deformed and plain low-alloy steel bars for concrete reinforcement*. West Conshohocken: ASTM International.
- Beeby, A. W. (2004). The influence of the parameter δ/ρ_{eff} on crack widths. *Structural Concrete*, 5(2), 71–83.
- Dang, L. B. (2009). *The study of crack width of HRB500 reinforced concrete members*. Zhengzhou University. (in Chinese).
- DL/T 5057-1996. (1996). *Design specification for hydraulic concrete structures*. China Electric Power Press. (in Chinese).
- DL/T 5057-2009. (2010). *Design specification for hydraulic concrete structures*. China Electric Power Press. (in Chinese).
- Du, M. M., & Su, X. Z. (2012). Study on the crack width at different positions of post-tensioned bonded prestressed concrete beams with 500MPa steel bars. *Journal of Building Structures*, 33(09), 141–147. (in Chinese).
- EN1992-1-1. (2004). *Euro-code2: Design for concrete structures-Part1: General rules and rules for building*. European Committee for Standardization.
- Frosch, R. J. (2002). Modeling and control of size face beam cracking. *ACI Structural Journal*, 99(3), 376–385.
- GB50010. (2010). *Code for design of concrete structures*. Chinese Building Press. (in Chinese).
- General Administration of Quality Supervision, Inspection and Quarantine; and National Standardizing Committee. (2007). "Common Portland cement." Chinese Standard GB 175-2007, Beijing, the People's Republic of China. (in Chinese)
- Guan, J. F., Zhao, S. B., Li, X. K., et al. (2011). Experiment and calculation method of crack width of reinforced concrete beams. *China Journal of Highway and Transport*, 24(5), 74–81. (in Chinese).
- Guan, J. F. (2010). *Research on theory and application of simulation model test for reinforced concrete structure*. Dalian University of Technology. (in Chinese).
- Guan, J. F., Liu, L. A., Bai, W. F., et al. (2020). Experimental study on the stiffness of 600MPa high-strength steel bars and high-strength concrete beams. *Journal of Applied Basic Science and Engineering*, 28(05), 1197–1211. (in Chinese).
- Guan, J. F., Liu, L. A., Zhang, Q., et al. (2021). Experimental study and calculation method of mid-span deflection of 600 MPa high-strength reinforced concrete beams. *Journal of Building Structures*, 42(08), 59–72. (in Chinese).
- Guan, J. F., Zhang, Q., Wang, W. S., et al. (2016). Resistance against cracking of reinforced concrete beams with 600MPa seismic steel bar. *Concrete*, 7, 49–52. (in Chinese).
- Guan, J. F., Zhang, Q., Wang, D., et al. (2018). Research on mechanical properties and constitutive model of 600MPa seismic steel bar. *Journal of Basic Science and Engineering*, 26(1), 122–131. (in Chinese).
- JTG D62-2012. (2012) *Code for design of highway reinforced concrete and prestressed concrete bridges and culverts*. China Communication Press. (in Chinese).
- JTJ267-98. (1998). *Design code for harbour engineering concrete structures*. China Communication Press. (in Chinese).
- Na, L. Y. (2006). *The experimental study on the crack behavior of concrete bending members reinforced with HRB400 steel*. Hunan University. (in Chinese).
- Li, X. K., Li, C. Y., Zhao, M. L., et al. (2019). Testing and prediction of shear performance for steel fiber reinforced expanded-shale lightweight concrete beams without web reinforcements. *Materials*, 12(10), 1–18.
- Li, Y. Y. (2007). *Experimental research on behaviors of reinforced concrete beams with 500MPa steel bars*. Tianjin University. (in Chinese).
- Li, Y. Z., Cao, S. Y., Liang, H., et al. (2018). Axial compressive behavior of concrete columns with grade 600 MPa reinforcing bars. *Engineering Structures*, 172, 497–507.
- Liu, P. (2012). *Experimental and Theoretical research on beams with HRB 500 high strength steel bars*. Hebei University of Technology. (in Chinese).
- Liu, Y. Y., Fan, Y. F., & Charis, A. (2019). Experimental study on flexural behavior of prestressed concrete beams reinforced by CFRP under chloride environment. *Advances in Civil Engineering*, 984, 230–238.
- Shang, S. Z. (2004). *Experimental study on flexural behavior of reinforced concrete beams with stiff and strong*. Shanghai University. (in Chinese).
- SL/T 191-2008. (2009). *Design code for hydraulic concrete structures*. China Water Power Press. (in Chinese)
- TB10002.3-2005. (2005). *Code for design of railroad reinforced concrete and prestressed concrete bridges and culverts*. China Railway Press. (in Chinese)
- Wang, M. P., Zhang, Z. Q., & Geng, S. J. (2007). Experiment of reinforced concrete simply supported beam with 500MPa ribbed carbon bars under bending. *Industrial Construction*, 37(8), 39–42. (in Chinese).
- Wang, X. L. (2007). *Experimental research on bend performance of RC beams with high-strength rebar*. Tianjin University. (in Chinese).
- Xiao, H. J. (2006). *Experimental research on bend behavior of HRB400 reinforced concrete beams*. Zhengzhou University. (in Chinese).
- Xiong, H., Ge, J., Feng, J., et al. (2018). Experimental study on the mechanical properties and service performance of HRB600 steel bars. *Journal of Building Structures*, 39(S2), 387–393. (in Chinese).
- Xu, F. B. (2007). *Experimental and theoretical research on flexural behavior of reinforced concrete beams with HRB 500 bars*. Hunan University. (in Chinese).
- Yao, X. H., Zhang, Y. L., Guan, J. F., et al. (2020). Experimental study and reliability analysis of flexural capacity of RC beams reinforced with 600 MPa grade steel. *Advances in Civil Engineering*, 2020(4), 1–26.
- Zang, P. (2007). *The experimental study on bending behavior of RC beams with 500MPa steel bar*. Hebei University of Technology. (in Chinese).
- Zhang, T. (2004). *The study of mechanical property of HRB500 reinforced concrete members*. Zhengzhou University. (in Chinese).

- Zhang, J. W., Li, C., Li, X. Y., et al. (2019). Experimental study on seismic performance of HRB600 reinforced high-strength concrete columns. *China Civil Engineering Journal*, 52(08), 6–17. (in Chinese).
- Zhang, J. W., Liu, J., Li, X. Y., et al. (2021). Seismic behavior of steel fiber-reinforced high-strength concrete mid-rise shear walls with high-strength steel rebar. *Journal of Building Engineering*, 42, 102462.
- Zhao, S. B., Guan, J. F., Zhang, X. P., et al. (2008). Statistical analysis and experimental study of crack patterns of reinforced concrete beams. *Engineering Mechanics*, 25(12), 141–146. (in Chinese).
- Zhao, S. B., Guan, J. F., Zhang, X. P., et al. (2009). Experimental study on effect of cross sectional depth of concrete beams on crack patterns. *Journal of Hydraulic Engineering*, 40(1), 88–93. (in Chinese).
- Zhu, E. Y., Li, D. D., Qi, M., et al. (2018). Experimental research on crack calculation of hydraulic RC beams with high-strength rebars. *SHUILIXUEBAC*, 49(05), 580–587. (in Chinese).

Publisher's Note

Springer Nature remains neutral with regard to jurisdictional claims in published maps and institutional affiliations.

Submit your manuscript to a SpringerOpen[®] journal and benefit from:

- ▶ Convenient online submission
- ▶ Rigorous peer review
- ▶ Open access: articles freely available online
- ▶ High visibility within the field
- ▶ Retaining the copyright to your article

Submit your next manuscript at ▶ [springeropen.com](https://www.springeropen.com)
